INVESTIGATIONS ON SURFACE ELECTRIC CHARGE OF SILICA NANOPARTICLES WITH DIFFERENT SURFACE ROUGHNESSES

A Thesis Submitted to
the Graduate School of Engineering and Science of
İzmir Institute of Technology
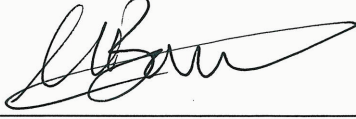in Partial Fulfillment of the Requirements for the Degree of

MASTER OF SCIENCE

in Mechanical Engineering

by
Büşra Öykü ALAN

December 2019
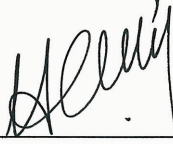**İZMİR**

We approve the thesis of **BÜŞRA ÖYKÜ ALAN**

Examining Committee Members:

_____
Assoc. Prof. Dr. Murat BARIŞIK
Department of Mechanical Engineering, İzmir Institute of Technology

_____
Prof. Dr. Mehmet POLAT
Department of Chemical Engineering, İzmir Institute of Technology

_____
Assist. Prof. Dr. Hasan ÇELİK
Department of Mechanical Engineering, İzmir University of Economics

19 December 2019

_____
Assoc. Prof. Dr. Murat BARIŞIK
Supervisor, Department of Mechanical
Engineering, İzmir Institute of
Technology

_____
Prof. Dr. Sedat AKKURT
Head of the Department of Mechanical
Engineering

_____
Prof. Dr. Mehtap EANES
Dean of the Graduate School of
Engineering and Sciences

ACKNOWLEDGMENTS

ABSTRACT

INVESTIGATIONS ON SURFACE ELECTRIC CHARGE OF SILICA NANOPARTICLES WITH DIFFERENT SURFACE ROUGHNESSES

Silica nanoparticles have been receiving more attention from diverse research areas recently due to their significant physical properties such as large pore volume and high internal surface area, colloidal stability, high biocompatibility, and tunable pore sizes. These silica nanoparticles are great candidates for drug delivery applications because they can transport a large amount of drugs into selective organs and tissues due to their high surface area and large pore volume. However, there are important drug delivery mechanisms that need to be understood properly such as cellular uptake, endosomal escape, drug loading and release, and crossing physical barriers. Physicochemical properties of nanoparticles (size, shape, surface charge, or surface chemistry) are important for understanding these mechanisms in order to develop successful drug delivery applications. This research investigates how these surface charge properties change with different particle, pore diameters, roughness structure on the nanoparticle surface, and different temperature and solution conditions. Also, we investigate how the surface charging behavior of rough nanoparticles interacts with a flat plate. Rough nanoparticles and their interactions with surfaces theoretical assumptions can be wrong and ionic distribution can show variation locally. In order to calculate ionic distribution and surface charge properties in these systems, proper equations and boundary conditions were employed. The charge regulation model was used as a boundary condition because of the electric double layer overlap effect. Results showed that there was a considerable variation on surface charge properties due to the roughness structure with different roughness and particle sizes and temperature difference.

Keywords and Phrases: *Surface charge density, charge regulation, silica nanoparticles, surface roughness, electric double layer overlap*

ÖZET

FARKLI YÜZEY PÜRÜZLÜLÜKLERİNE SAHİP SİLİKA NANOPARTİKÜLLERİN YÜZEY ELEKTRİK YÜKÜ ÜZERİNE ARAŞTIRMALAR

Silika nanopartiküller yüksek iç yüzey alanı ve geniş gözenek hacmi, yüksek biyo-uyumluluk ve kolloidal kararlılık gibi avantajlı fiziksel özellikleri ile çeşitli biyomedikal uygulamalar için uygun adaylardır. Özellikle ilaç iletimi uygulamalarında yüksek ilaç taşıma kapasitesi sayesinde sıklıkla tercih edilirler. Silika nanopartiküllerin yüzey elektrik şarjı bu uygulamaların verimliliği açısından çok belirleyicidir. Çünkü ilaç iletimi uygulamaları sırasında görülen bazı hücre içi mekanizmalar nanopartikülün yüzey elektrik şarjına bağlıdır. Örnek olarak, ilaç iletiminin başarısını fazlasıyla etkileyen hücresel alım mekanizması nanopartikülün yüzey elektrik şarjı ve boyutları ile doğrudan ilişkilidir. Ayrıca ilaç iletimi sırasında görülen en önemli sorunlardan birisi de endozomal kaçışın sağlanmasıdır. Nanopartikül yüzey elektrik şarjı ve boyutunun endozomal kaçışın sağlanmasında etkili olduğunu gösteren çalışmalar vardır. Bu nedenle yüzeyi pürüzlü nanoparçacıkların yüzey elektrik şarjının incelenmesi önemli bir konu oluşturmaktadır. Bu çalışmada yüzeyi gözenekli nanopartiküllerin farklı pürüz ve parçacık çapları, farklı solüsyon özellikleri, sıcaklık değişimi ve düz bir yüzey ile etkileşimi sonucunda oluşan yüzey elektrik şarjı davranışı incelenmiştir. Yüzeyi pürüzlü nanopartiküllerin yüzeyinde oluşan iyonik dağılım ve elektrik şarjı davranışının doğru olarak hesaplanabilmesi için uygun denklemler ve sınır şartları seçilmiştir. Elektriksel çift tabakaların çakışması etkisinden dolayı sınır koşulu olarak kullanılan yük regülasyon modeli nanopartikül yüzeyinde sınır şartı olarak seçilmiştir. Sonuçlar, farklı pürüzlülük ve parçacık ebatları ve sıcaklık farkına sahip pürüzlülük yapısı nedeniyle yüzey yükü özelliklerinde önemli bir değişiklik olduğunu göstermektedir.

Anahtar Kelimeler ve Deyimler: *Yüzey yükü yoğunluğu, yük regülasyonu, silika nanopartiküller, yüzey pürüzlülüğü, elektriksel çift tabakaların çakışması*

TABLE OF CONTENTS

LIST OF FIGURES

LIST OF TABLES

LIST OF SYMBOLS

C_{i0}	Bulk concentration of ith ion	
C_{KCl}	Bulk concentration of KCl	mM
D_i	Diffusivity of ith ion	m^2 / s
E	Electric field	N / C
F	Faraday constant	C / mol
K_A, K_B	Equilibrium constants	
N_{total}	Total number of the site functional groups	$sites / nm^2$
pH	pH level	
D_R	Diameter of roughness	nm
D_P	Diameter of particle	nm

Greek Letters

ε_0	Relative permittivity of vacuum	F / m
ε_r	Relative permittivity of ionic liquid	F / m
σ_s	Surface charge density	C / m^2
λ	Debye length	nm
ψ	Electric potential distribution	V / m
Γ	Surface site density	$sites / nm^2$
λ_j	Limiting ionic conductivity of jth ion	$S \times cm^2 / mol$

Subscripts

s	Surface
R	Roughness
P	Particle
Flat-Plate	Flat surface
Flat-Theory	Flat theory
Rough-Particle-Ave	Rough nanoparticle

CHAPTER 1

INTRODUCTION

In recent years, mesoporous silica nanoparticles (MSN) have become more popular nanomaterials because of their physical and structural properties such as high colloidal stability, high biocompatibility, high internal surface area, and large pore volume and tunable particle and pore sizes. Because of their unique properties, MSNs are also great candidates for diverse biomedical applications such as bio imaging for diagnostics[1,2], bio sensing[3], bio catalysis[4,5], drug delivery[6–8], gene delivery[9], and anticancer therapeutic agents[10]. Surface charge properties of mesoporous silica nanoparticles play a significant role in all these applications but detailed interpretations about the influence of surface properties of MSN on biomedical applications does not exist in the literature.

Generally, MSNs have diameters less than 500 nm and their pore sizes range between 2-50 nm and can be produced with desired geometrical features using different synthesis methods. Mesoporous structures such as pore size distribution and porosity can be arranged for the specific type and amount of drugs. MSNs can be synthesized using the sol-gel method and spray drying method. These nanoparticles are great candidates for drug delivery systems as they can transport a large amount of drugs due to their high surface area and large pore volume and they have high loading capacity. Especially, MSNs are suitable for targeted drug delivery applications because nanoparticles can be designed to deliver to specifically targeted cells and load the proper type and amount of drug. In targeted drug delivery medicine is only delivered to targeted and specified cells or tissues. This improves efficiency and reduces side effects. For instance, targeted drug delivery systems are very promising and groundbreaking developments for cancer treatment therapies. In cancer treatment, it is possible to directly deliver the medicine to the targeted cancer cells. MSNs need to be designed and synthesized with specific surface features that are suitable for a significant drug delivery system.

The importance of electric charge of an MSN can be explained by some of the major mechanisms of the targeted drug delivery. First, drug loading-releasing mechanisms depend on surface charge, in addition to mesoporous structures and pore

sizes. Second, cellular uptake is determined by the surface charge. Studies reported that 100-150 nm nanoparticles are more efficient for cellular uptake by comparison to 50-55nm MSNs[11,12]. The surface charge depends on the nanoparticle size; a decrease of nanoparticle diameter increases the absolute charge value[13]. Third, endosomal escape was found to depend strongly on surface charge. When endosomal escape cannot be achieved this may cause disruption of nanoparticles and drugs with digestive enzymes. Endosomal escape is very important for the efficient delivery of nanoparticles[14]. There are some strategies to achieve an endosomal escape. Studies reported that MSNs with negatively charged surface properties achieve endosomal escape more easily[15]. Fourth, protein corona forming on nanoparticle by the coverage of biomolecules (such as proteins, sugars, and lipids) is directly related to the surface charge[16]. The protein corona has a dynamic structure and it defines the identity of the nanoparticle[17]. The presence of a protein corona modifies the surface properties and changes the hydrodynamic diameter and the electrokinetic properties of the nanoparticle. Considering all these reasons, it is important to analyze the mesoporous nanoparticles' surface charge, zeta potential, electric double layer (EDL) and electrokinetic interactions of MSNs and their dependence on structural MSN parameters such as size, porosity and surface condition.

Surface charge is a natural reaction that occurs when a solid surface interacts with an aqueous media. Due to the protonation/deprotonation reactions on the surface and adsorption of ions, surface charge occurred in a solid/liquid interface. The charged surface attracts counter-ions and repels co-ions and Electric Double Layer will be formed on the surface. EDL structure changes the ionic distribution on the surface. Generally, ionic distribution on the surface can be explained with Boltzmann-Distribution (BD), but this simplification is only useful under these assumptions: zeta potential must be smaller than 25 mV and surface must be flat and sufficiently far away from any other bodies. For nanoscale roughness and these nanosystems, these assumptions are wrong and using Boltzmann-Distribution simplification is inappropriate. Instead of the BD, Nernst-Planck equation can be used for defining ionic transport or the Poisson equation can be used to identify the electric distribution. These equations can be solved together for calculating electric distribution through EDL.

Recent techniques allow the production of various forms of MSNs with easy to control the size, and surface condition. In Figure 1.1, particle size variation at two different surface conditions (Figure 1.1a-j) [18] is presented from the study of Koike et al., while the variation of the surface condition at a given particle size can also be obtained

as shown by Kang et al. (Figure 1.1k-n)[19]. For such nano-systems, particle size and surface condition determine the ionic concentration and the resulted zeta potential at the surface. First, a decrease in overall particle size develops curvature effects that cause ionic condition around the particle to diverge from a flat surface. The curvature effect is formed due to the decreased surface to volume ratio by the decrease in particle diameter[20]. Second, surface structures of either naturally developed or engineered surface patterns or roughness EDLs of opposing surfaces overlap, and ionic distribution shows local variations and differs from existing flat surface theory. For a nanoparticle roughness forming from valleys and hills, ionic layers in valleys extending from opposite surfaces will overlap when the spacing between is smaller than the EDL thickness. Further curvature effects will also develop at the hills of the surface roughness. Due to all these complications, assuming a constant surface zeta potential as a material property independent of nano-system's conditions yields in very inaccurate results.
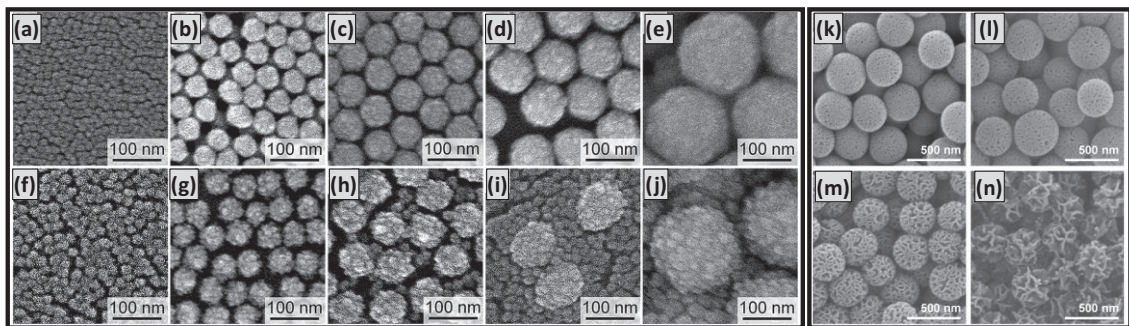
Figure 1.1. Different size ((a&f) 12nm, (b&g) 44nm, (c&h) 60nm, (d&i) 88nm, and (e&j) 170nm) silica nanoparticles with flat (a-e) and rough (f-j) surface conditions developed in Koike et al. (Source: 18) - Published by The Royal Society of Chemistry. (k-n) Various surface conditions of wrinkled silica nanoparticles obtained in Kang et al. (Source: 19) - Published by The Nature Publishing Group.

In order to properly calculate the nano-particle surface charges in nano-systems, ionic diffusion equations must be solved as Poisson-Nernst-Planck (PNP) equations without Boltzmann simplification. Furthermore, the PNP solution using a constant surface charge or constant potential boundary conditions still cannot calculate the real physics of nano-systems. Electrical charging of the surface is the result of

protonation/deprotonation reactions at the solid/liquid interface and occurs as a function of ionic density that formed on the surface. In this case, the surface charge is a function of ionic distribution that formed as a function of the surface charge itself. According to this, the surface charge and EDL need to be solved together. Also, "Charge Regulation (CR)" represents such occurrence of EDL overlap and can model the natural behavior of surfaces. Ninham and Parsegian[21] identified the charge regulation behavior of surface chemistry the first time in the literature. After that, charge regulating behavior of surfaces investigated by several studies through surface force measurements by colloids[22,23] and AFM[24,25] experiments. From that time, researchers started to implement the charge regulation model into numerical calculations with using proper charging models as a boundary condition. In recent years, CR models have become very popular in many research fields such as colloidal chemistry and atomic force measurement (AFM) methods[26,27].

In a previous study, surface charge distribution investigated through surfaces with nanopatterned roughness using CR and active charge model as a boundary condition[28]. This study found that surface charge is dependent on the size of the nanopatterned structure on the surface. Also, curvature and EDL overlap effect was observed as the roughness forms on the nanopatterned structure. This representative nanopattern is made of repeating circular pits and tips of identical size. In the pits of the surface pattern, surface charge density is decreasing due to the increasing EDL overlap effect, while surface charge density is increasing due to the developed curvature effect at the tips of the structure. There is an experimental study showing that surface charge density behavior varies with the curvature of the nanoparticle[20]. Researchers found that the surface charge density of particle decreases with increasing particle size. Surface charge density values show a rapid decrease in the size range between 4.1 and 30 nm and shows an independent behavior for particle size values larger than 30 nm due to the curvature effect of the nanoparticle. Also, these experimental values[20] show similar behavior with numerical values[13] which is calculated on the previous study that is related size and curvature dependency of surface charge of the nanoparticle.

On the other hand, temperature variation is also important in electrokinetic phenomena occurring at micro/nanoscale applications. Physical properties of both the surrounding liquid medium and the particle surface are temperature-dependent on a solid-liquid interface. Temperature difference influences the ionic transport due to the varied ionic mobilities and temperature variation is also effect surface properties of a

nanoparticle which has a significant impact on nanoparticle electrolyte interactions at the micro/nanoscale[29–31]. Ionic concentration and pH level of an electrolyte solution, type and charge of the ions, number of binding sites on the nanoparticle surface and equilibrium constants of the surface reactions are influenced by the temperature variation at the nanoscale interactions.

In the literature, the relation between temperature variation and electrostatic properties of a silica surface has been observed and investigated in several studies. Temperature variation is a desirable and useful state for some studies which is like thermal gates. The thermal gate modulates the ionic transport with varied temperature and it is more effective than other gating mechanisms. However, temperature variation can be a problem for some other applications such as capillary electrophoresis because electrophoretic motion is influenced by temperature variation due to the Joule heating effect[31,32]. According to previous studies, the surface charge of a silica surface increases with an increased temperature. But, surface charge behavior of silica surface is affected by different geometrical aspects like the spherical shape of a nanoparticle or roughness geometries on its surface. Roughness structure on the surface which includes hills and valleys changes the ionic distribution and surface charge locally. Due to that temperature effect on particles, surface charge needs to be examined for rough spherical nanoparticles.

In addition to that, surface charging properties of nanoparticles are very important when the nanoparticle is interacting with another dielectric entity such as particle or surface. Because the surface charge is highly affected during the interaction of two dielectric entities. When the distance between two charged objects is shorter than the electric double layer thickness, electric double layers of these charged entities will overlap. For this reason, ionic concentration in the interaction region between two interacting surfaces will be different than when there is no interaction between charged entities. There is a nonuniform surface charge distribution around these interacting objects according to different ionic concentrations. In the literature, there are additional studies that examined whether surface charge properties of two interacting surfaces remain constant. Surface charging behavior of nanoparticle when interacting with another object is important for colloidal stability, biomolecular transport, and drug delivery.

The aim of this study is to investigate the surface charging behavior of a rough nanoparticle under different conditions such as pH, concentration, different particle, and roughness parameters and temperature variation.

The outline of this study can be summarized as follows; In Chapter 2, a comprehensive literature survey on mesoporous silica nanoparticle applications, intracellular mechanisms, and importance of investigating the charging behavior of rough nanoparticles under different surface conditions such as roughness, temperature, and interaction effects will be given. In Chapter 3, a formulation of the problem will be discussed. In Chapter 4, the computational domain used for numerical calculations, and related details will be presented. In Chapter 5, the results of surface charge variation of rough nanoparticle examined under pH, solution concentration, roughness, temperature, and interaction effects. Lastly, in Chapter 6, the study will be summarized and appropriate conclusions will be made.

CHAPTER 2

LITERATURE REVIEW

MSNs were discovered about 20 years ago by researchers at Mobil[33,34] and they have a hierarchically ordered porous system. MSNs have been used as a host material for therapeutics due to their high loading capacity and protection of the guest molecules with their porous structure since 2001. MSNs with different particle sizes and pore geometries can be obtained by using different synthesis techniques. Sol-gel processes and spray drying methods are the most commonly used synthesis techniques for producing various types of MSNs. For example, MCM (Mobile Crystalline Materials)-41 is one of the most widely used type of MSNs for drug delivery systems. MCM-41 has a hexagonal structure and consists of 2.5 to 6 nm pores[35,36]. MCM-48 has a cubic structural geometry but MCM-50 has a lamella-like structures[37]. For instance, SBA-15 used for a diverse biomedical application due to its ordered porous structure. This nanomaterial is named Santa Barbara Amorphous (SBA) type nanomaterial because it was first discovered by The University of California, Santa Barbara. Different types of SBA materials can be synthesized as SBA-11 (cubic), SBA-16 (cubic-cage structured), SBA-15 (hexagonal) and SBA-12 (3D hexagonal), according to symmetrical geometry of the porous structure. SBA nanomaterials have different physical properties from MCM nanomaterials because their thickness of silica walls[38] is denser and pore sizes are larger (4.6-30 nm). In addition to that, various other nanoparticles have mesoporous structures can be synthesized with changing reaction parameters such as solution concentrations and pH value, chemical nature of the surfactants and time. With fine-tuning reaction parameters, morphology, size and pore structure of mesoporous silica can be adjusted precisely. For instance, there are studies that virus-like mesoporous silica nanoparticles synthesized with bio mimicking of unique surface morphology of virus surfaces in the literature[39,40]. The unique mesoporous silica nanoparticles with a spiky tubular rough surface show highly efficient cellular internalization. Roughness structure on the virus-like mesoporous silica formed by nanotubular structure is similar to the rough surface on viruses consisting of spiky proteins[39]. Due to that roughness structure on the surface, great cellular internalization and efficient blood circulation time can be achieved.
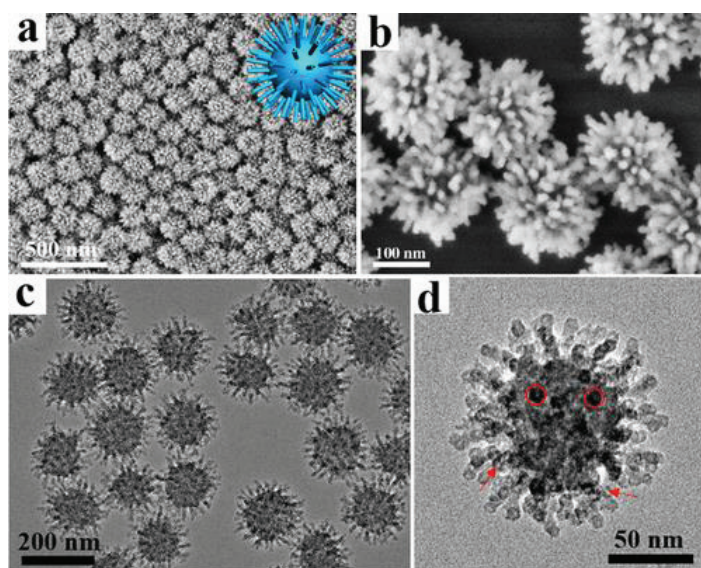
Figure 2.1. (a, b) SEM and (c, d) TEM images of virus-like mesoporous silica nanoparticles (Source: 37)

2.1. MSNs Application Areas

Mesoporus silica nanoparticles are promising for diverse biomedical application (bio imaging for diagnostics[1,2], bio sensing[3], bio catalysis[4,5], drug delivery[6–8], gene delivery[9], and anticancer therapeutic agents[10]) but especially, MSNs are very favorable for drug delivery applications due to their unique properties. This includes good biocompatibility, high drug loading capacity and efficient encapsulation of drug molecules. Also, MSNs surfaces can be easily functionalized and it is important for interactions with other surfaces and colloidal stability. MSN surfaces specifically modified to provide targeted cell-targeting or load a proper type and amount of drug. It is important that medicine is delivered to only specified and targeted cells during targeted drug delivery. Owing to that, efficiency of drug delivery applications can be increased, side effects on the healthy cells can be reduced and the proper type and amount of drug can be delivered to the targeted cells. For instance, targeted drug delivery systems are very promising and groundbreaking developments for cancer treatment therapies. In cancer treatment, it is possible to directly deliver the medicine to the targeted cancer cells. MSNs need to be designed to (i) enter only the targeted type of cell, (ii) carry the required

amount of drug, and (iii) remain inside the cell long enough to release the required drug without being destroyed. MSNs must be synthesized with specific surface features that are suitable for a significant drug delivery system.

2.2. Intracellular Mechanisms

During drug delivery application there are some important intracellular mechanisms which occur related to physicochemical properties of nanoparticles such as particle size, shape, surface chemistry, surface charging, and surface roughness. These intracellular mechanisms such as cellular uptake, endosomal escape, protein corona formation, crossing some physical barriers (Blood-Brain Barrier) and drug loading-releasing mechanisms, occur during drug delivery and have an important influence on the efficiency of these applications. In the literature, there are studies examining the relationship between surface properties of nanoparticles and drug delivery mechanisms. For instance, cellular uptake size and surface features of nanoparticles are becoming very important.

Surface modifications (hydrophobic/hydrophilic and being positive/negative charged) are important for loading appropriate drug type. Surface charge and zeta potential of nanoparticles have great importance for nanoparticle-cell interactions. Nanoparticles can be transported through the cells with endocytosis or exocytosis. Cellular uptake is a two-step process: binding and internalization. During cellular uptake nanoparticles will interact with the cell membrane and cell membrane is covered by negatively charged molecules (glycocalyx)[16]. Accordingly, cell membrane is generally considered negatively charged. Surface charge of nanoparticle and cell membrane is important during cellular uptake because electrostatic interactions determine the nanoparticle cell interactions. There are studies that positively charged nanoparticles more easily internalized than the negatively charged or neutral ones[41]. This behavior can be related to specific electrostatic features of nanoparticle and negatively charged nature of the cell membrane. Also, the size of the nanoparticle is affected by cellular internalization. For instance, recent studies concluded that 50 nm is an optimum size for an efficient cellular internalization than the larger (100-280 nm) and smaller (30-25 nm) ones[42,43]. Also, there are other studies suggesting that 100-150 nm nanoparticles are more efficient for cellular uptake by comparison to 50-55 nm nanoparticles[44,45]. Surface charge

variation with different particle sizes explained by the previous study and suggesting that the decrease of nanoparticle diameter increases the absolute charge[13]. Endosomal escape is also a significant mechanism during drug delivery because when endosomal escape couldn't be achieved in a proper time, it can be caused by the degradation of nano-carriers and their cargo molecules in an endosome. Nanoparticles enter the cell with endocytosis and then reach endosomes using the endosomal pathway. However, nanoparticles and their cargo molecules can be entrapped in an endosome and destroyed with digestive enzymes. There are some strategies in nature for achieving endosomal escape easily. Studies showed that the ability of endosomal escape and electrostatic properties of nanoparticles are related to each other. For instance, they suggested that negatively charged MSNs achieve endosomal escape more easily[46]. On the other hand, efficient cellular uptake and endosomal escape are not enough for successful drug delivery implementation because the surface charge of nanoparticle also affected by protein corona formation. When a nanoparticle enters a biological media its surface covered by some biomolecules such as protein, sugar, and lipid. Protein corona formation is modifying the surface properties and defines the identity of the nanoparticle[16,17]. This structure on the nanoparticle surface changes the electrokinetic properties and it is important for nanoparticle cell interactions[47]. Also drug loading and releasing mechanisms related to surface charge and electrokinetic features of nanoparticles. Blood circulation time is an important factor for drug delivery because the compound needs to circulate in blood long enough to delivered successfully[48]. Some studies said that small particle size related with long blood circulation time[11,12].

In conclusion, understanding the underlying mechanism of these intracellular mechanisms and their relation with physicochemical properties (size, shape, zeta potential, surface charging, and surface geometry) of nanoparticles is important for achieving successful biomedical applications.

2.3. Temperature Effect

Physical properties of both the surrounding liquid medium and the particle surface are temperature-dependent on a solid-liquid interface. There are several studies that examined this relationship between temperature difference and electrostatic properties of micro/nanoscale devices.

For instance, in electrophoresis applications, there are several important factors which are particle properties, ionic media and applied electric field. In addition to these factors, temperature is also important for electrophoresis applications. The physical properties of the particle surface and the surrounding liquid medium are also temperature-dependent. The electrophoretic behavior of the particle is influenced by temperature due to the Joule heating effect. Temperature and Joule heating effect on the electrophoretic behavior of a particle is investigated in many studies. For example, Evenhuis and Haddad[49] found that the magnitude of the applied electric field and geometrical properties such as length and the radius of a device are effective on heat dissipation during electrophoresis. After that, the importance of the thickness of the electric double layer on the Joule heating effect was observed by Seyrek[50]. The temperature effect was investigated on capillary electrophoresis and calculated theoretically by Wang and Tsao[51]. They observed that sample velocity can be increased by the Joule heating effect due to the variation of mobilities of ions according to the heating effect. This behavior was experimentally investigated and observed by Evenhuis[52]. Also, the performance of capillary electrophoresis was simulated by Tang[32] when the Joule heating effect had occurred, then they observed that thermal effect had an influence on sample concentration behavior. The importance of the Joule heating effect by Xuan and Li[53] on the electric current and the separation efficiency was investigated. Research showed that temperature increases during the electrophoresis due to the Joule heating effect and the temperature range was dependent on the experimental conditions. Joule heating occurred during capillary electrophoresis when an electric field was applied through the electrolyte solution. Joule heating affected electroosmotic flow and sample transport and separation due to the formed temperature gradient. During electrophoresis, the viscosity and the permittivity of the liquid medium, the diffusivity of ionic species and surface reactions on a particle surface were temperature dependent. The temperature increased and temperature gradient was formed due to the Joule heating effect. Joule heating effect is dependent on capillary length, the strength of the applied electric field and the concentration of the background ionic media.

In the literature, there are micro/nanoscale implementations that temperature difference is observed and used for a purpose. For instance, in thermal gates temperature difference applied by heating up the nanochannel surface and which is used for arranging the ionic transport[29]. Compared to other gating mechanisms thermal gate manages ionic transport more efficiently. The temperature difference is very important for the ionic

mobilities of ions that dissolved in the electrolyte solution. Therefore, ionic properties and electric current of the electrolyte solution are depending on the temperature difference. At the micro and nanoscale, when the temperature difference occurs ionic mobilities of dissolved ions will be increased and surface chemistry of surfaces will be modified. As a result, ionic transport on micro or nanoscale applications is effected by temperature variation[29–31]. When the temperature of the silica surface increases, surface charge behavior of silica surface shows an increasing behavior. After that, the silica surface starts to attract more counter-ions due to the increased surface charge. Accordingly, ionic mobilities of the ions that dissolved in the ionic solution started to increase. This increasing behavior of ionic mobilities provides efficient ionic transport in nanoscale devices due to the increased temperature. Also, with an increased temperature, equilibrium constants of the surface chemical reactions at the silica surface will be changed. The temperature difference will affect surface charge properties of silica surface according to changing surface chemistry and solution properties such as relative permittivity and ionic mobilities.

The temperature effect is investigated also for salinity gradient power systems. Salinity gradient power is a promising renewable energy method that is used for producing electrical energy using the mixing process through (NRED)[54] and transferring Gibbs free energy of this process. A salinity gradient is connecting two large reservoirs containing different salt concentrations by a Nanopore. Ions move through from the high salt concentration reservoir drive to the low salt concentration reservoir by a salt gradient. In the literature, the thermal sensitivity of the salinity-gradient-driven energy conversion process performed through reverse electrodialysis is investigated previously. Because ionic transport depends highly on the temperature and salinity gradient power mostly depends on ionic transport. When the temperature is increasing, the surface charge density of mesopores shows an increasing behavior due to an increased zeta potential of the pore walls.[55] The ionic mobility also increases with increasing temperature according to a decrease in the liquid viscosity. According to these reasons, the thermal dependence of efficiency of the salinity gradient power systems is important.

Due to that temperature effect on particles, surface charge needs to be examined for porous spherical nanoparticles. In our study, we model silica nanoparticles with roughness on its surface and investigate the temperature effect on its surface.

2.4. Surface Charge and EDL

Surface charge is a natural reaction that occurs when a solid surface interacts with an aqueous media. Due to the protonation/deprotonation reactions on the surface and adsorption of ions surface charge occurred in a solid/liquid interface. Surface charge is dependent on electrolyte concentration, pH and ionic distribution. The charged surface attracts counter-ions and repels co-ions and Electric Double Layer will be formed on the surface by this behavior. EDL structure changes the ionic distribution on the surface. Due to that, there is a relation between EDL and surface charge. Generally, ionic distribution on the surface explained with Boltzmann-Distribution but this simplification can be useful under these assumptions: zeta potential must be smaller than 25 mV and surface must be flat and sufficiently far away from any other bodies. The electric charge of the surface can be calculated analytically with using these assumptions and Poison-Boltzmann model. For nanoscale roughness and these nanosystems, these assumptions are wrong and using Boltzmann-Distribution simplification is inappropriate. Because by decreasing particle size, the surface will be rounded, and when the distance between the particle and other surfaces is less than the thickness of the ionic layer, ionic layers on the opposite surfaces will overlap. In nano-scale systems, surface charge calculations that depend on Poisson-Boltzmann are invalid for these reasons. Due to the fact that there is not an applicable model, a large scale of the literature ignores these facts and continues to use the PB model in nano-systems. Also, the flat surface assumption is not applicable to real life. In nature, there are varying topologies and roughness structures on the surfaces. Because of that roughness structure, an electric double layer overlap will occur on the surface and ionic distributions will be different from BD.

Roughness geometries on the nanoparticle surface create two different geometrical forms such as valleys and hills. The ionic distribution will deviate from Boltzmann Distribution on these geometrical forms. For example, in valleys ionic layers that extending from close surfaces approaching each other will overlap because the spacing between is smaller than the EDL thickness. Ionic distribution on the surfaces of valley structures will be different due to the overlap effect. Also, in hills, curvature effect will occur due to the decreased surface to volume ratio and increased diameter. There are some studies that mentioned about curvature effect previously[13]. The surface charge of a

rough nanoparticle will show local variation as a function of roughness due to these geometrical differences.

According to that, instead of BD, the Nernst-Planck equation can be used for defining ionic transport. The Poisson equation gives the electric distribution and these equations can be solved together for calculating electric distribution through EDL formed on a rough nanoparticle. In order to calculate the nano-particle surface charges in nano-systems, ionic diffusion equations must be solved as Poisson-Nernst-Planck (PNP) equations without Boltzmann simplification.

2.5. PNP and Charge Regulation Model

There are analytical and numerical solutions of PNP, but boundary conditions applied in existing studies can not calculate the real physics of nano-systems. In general constant surface charge or constant potential used as boundary conditions in solutions. In contrast to these mathematical assumptions in real surface physics, both electric surface charge, and potential show variation. Basically, electrical charging of the surface is the result of protonation/deprotonation reactions at the solid/liquid interface and occurs as a function of ionic density that formed on the surface. In this case, the surface charge is a function of ionic distribution that formed due to this surface charge and these two physics needs to be solved together. For rough nanoparticles and their interactions with other surfaces, a Charge Regulation model needs to be used for a boundary condition on a nanoparticle surface. Because both constant surface charge and constant electric potential assumptions are insufficient in this type of system.

The Charge Regulation model was described by Ninham and Parsegian for the first time in the literature[21]. The Charge Regulation model has been used in several studies using active charge models as a boundary condition of surface for numerical studies. For instance, the Charge Regulation model in the electric double layer is very important for diverse application areas such as colloidal chemistry, ion adsorption, interparticle forces and atomic force measurement (AFM) studies[56,57]. The Charge Regulation model is examined in several studies such as surface force measurements by colloids[22,23] and AFM[24,25]. Charge regulation description is used when overlapping double layers are mentioned. Because surface charge density strongly varies with electrolyte solution conditions such as pH or ionic concentration. When EDL's are overlapping ionic

properties are changing and the surface charge is regulating according to different solution conditions. Using force measurements with the surface forces apparatus (SFA) or AFM[58,59] studies Charge Regulation model can be observed. Generally, in these studies, the flat surface is used to determine surface charge by applying force measurements through the known surface location. During AFM force measurements there is an EDL overlapping occurs between the AFM tip and the surface. In the literature, there are limited studies that are considered surface heterogeneity for rough surfaces, but there is not a proper explanation about surface charge behavior of rough surfaces. In nanoscale applications surface charge density of a surface calculated as a local ionic property. The charge regulation model used as a boundary condition of surface and surface charge density numerically calculated using this boundary condition.

Charge regulation calculates the protonation/deprotonation effects of surface reactions on the particle surface. There are several studies that investigating surface charging behavior of surfaces in channels[60,61]. In these studies, EDL overlap occurs and ionic distribution changes locally on the surface. Also, there a few studies that mention surface geometry effects on surface charge density[58,59], but proper identification cannot determine about surface roughness effects on surface charging.

Since charge regulation is used when EDL's overlapped, this behavior occurs between two charged colloidal and spherical particles. In such systems, interactions are explained with the theory of Derjaguin, Landau, Verwey, and Overbeek (DLVO), these interactions affected by van der Waals and electric double layer forces. When two electric double layers are getting close to each other, the overlap of electric double layers modifies the local ionic environment. In this situation Charge regulation model used as a boundary condition of colloidal particle.

2.6. Interaction with a Flat Plate

When a nanoparticle immersed in an ionic liquid nanoparticle surface will be charged due to the surface chemical reactions at the solid/liquid interface. Surface charging behavior of silica nanoparticle in an ionic media is important for different research areas such as colloidal chemistry, electrokinetic transport of species at micro or nanoscale devices, biomedical applications, drug delivery, and surface chemistry. The surface charge of the silica surface will change when the nanoparticle is interacting with

another surface. For instance, during drug delivery applications nanoparticle will interact with cell surface to provide cellular uptake. Cellular uptake is an important process for efficient drug delivery applications. Electrostatic properties of both charged nanoparticle and charged cell surface are important during cellular uptake. There are several studies showing the effect of the charge properties of nanoparticles on cellular uptake when the nanoparticle is interacting with the cell surface. Also, charging behavior between spherical silica particles are important for colloidal stability. Electrokinetic transport of ions or particles influenced by surface charging behavior of particle and silica surface in nanoscale devices. The surface charging behavior of the surface is related to the electrostatic properties of particles in an ionic solution. If the charged surfaces are closer to each other electric double layers growing from opposite surfaces will overlap and ionic solution concentration will change according to that. When a silica nanoparticle is interacting with a flat surface in an ionic solution there is a different ionic concentration that occurs in the interaction region between surfaces. Ionic concentration in the interaction region between surfaces is very different from a non-interaction case. Accordingly, there is a non-uniform surface charging behavior is formed on the nanoparticle surface when interacting with other surfaces. In contrast, there are several studies considering surface charging behavior of interacting surfaces as constant. For instance, surface charge densities of interacting surfaces assumed constant in the well-known Derjaguin, Landau, Verwey, and Overbeek (DLVO) theory. Also, generally flat surface was used in these studies, there has not been a proper explanation regarding the surface charging of rough nanoparticle when interacting with surfaces.

CHAPTER 3

THEORETICAL BACKGROUND

When a solid surface meets with an ionic liquid there is a protonation/deprotonation reactions occurring on the solid/liquid interface. The surface will be charged due to surface chemical reactions and adsorption of ions, then there is an ionic distribution that will be formed on the surface. Generally, ionic distribution on the surface can be defined with the Boltzmann distribution (BD)[62–64]. The Poisson equation gives an electric potential distribution and the electric potential distribution through the electric double layer can be calculated by combining the Poisson equation and Boltzmann Distribution. According to that, the Poisson-Boltzmann (PB) equation is obtained. Poisson Boltzmann equation can be solved analytically with using The Debye-Hückel simplification[65] when the electric potential of surface lower than 25 mV. However, when the electric potential of surface higher than this value this simplification cannot be used anymore. Boltzmann Distribution is only applicable under these assumptions; the surface must be flat and sufficiently away from any other surfaces and there is an infinitely extending EDLs occurred on the surface, the electric potential of the surface must be lower than 25 mV. However, when opposite surfaces getting closer to each other EDLs growing from opposite surfaces start to overlap, ionic distribution will change locally and using Boltzmann distribution with Poisson equation is wrong for this type of case. In the EDL overlapping case, electric potential through the surface differs from the non-overlapping case and ionic distribution through EDL deviates from Boltzmann distribution. For this case, instead of Boltzmann Distribution, the Nernst-Planck equation should be employed to calculate ionic mass transport. Therefore, Poisson-Nernst-Planck (PNP) equations can be applicable for calculating surface charge for EDL overlapping cases. Also, in the case of EDL overlap using proper boundary conditions on the surface is very important for calculations. In the literature, constant surface charge[66,67] or constant potential[68] is used as a boundary condition on the surfaces when solving PNP equations. However, using constant surface charge or potential as a boundary condition cannot explain the real physics of the surface clearly. Electric potential and surface charge

density on the surface are affected by each other and there is an equation that shows the relation between them (Equation 3.1).

$$-\varepsilon_0 \varepsilon_r \vec{n}.\nabla \psi = \sigma_w \qquad (3.1)$$

When constant surface charge density is assumed on the surface, the electric potential value at the surface shows variation due to the EDL overlap. In contrast to that, if a constant electric potential condition is employed on the surface, the surface charge density of the surface will change due to the EDL overlap. Using these boundary conditions cannot give the real behavior of the surface because there is a non-uniform ionic distribution will occur on the surface due to the surface chemistry. Surface charge and electric potential show variation according to local ionic distribution, both of them cannot remain constant. According to that charge regulation model need to be employed on the surface to model this charging behavior. The charge regulation model considers the variation of surface charge with surface chemical reactions, adsorption of ions and electrolyte solution conditions. In this study, the charge regulation model is employed on the surface because for nanoparticles and their interaction with surfaces PNP equations need to be solved with proper boundary conditions.

In this model, a rough silica nanoparticle with diameter D_P with roughness (D_R) structure on its surface is considered. The liquid phase is considered as KCl (i.e. symmetric 1:1) aqueous electrolyte solution consists of 4 types of ionic species namely; H^+, K^+, Cl^- and OH^- ions with their bulk values being c_{10}, c_{20}, c_{30}, and c_{40}, respectively. When silica nanoparticle is in contact with an electrolyte solution its surface is charged due to protonation/deprotonation of ions. The surface charge is mostly dominated by the K^+ and Cl^- ions and the pH level of the solution is adjusted by the H^+ and OH^- ions.

There are two fundamental dissociation/association reactions occurred at the solid/liquid interface as follows:

$$SiOH \leftrightarrow SiO^- + H^+ \qquad (3.2)$$

$$SiOH + H^+ \leftrightarrow SiOH_2^+ \qquad (3.3)$$

The equilibrium constants can be calculated by using:

$$K_A = \frac{\Gamma_{SiO^-}[H^+]_w}{\Gamma_{SiOH}}, \quad K_B = \frac{\Gamma_{SiOH_2^+}}{\Gamma_{SiOH}[H^+]_w} \tag{3.4}$$

where Γ_{SiO^-}, Γ_{SiOH} and $\Gamma_{SiOH_2^+}$ are the surface site densities of SiO⁻, SiOH and $SiOH_2^+$, respectively and $[H^+]_w$ is the hydrogen concentration at the solid/liquid interface. The surface charge density of the silica surface can be defined as:

$$\sigma_w = -\frac{F\Gamma_{total}}{N_A} \frac{K_A - K_B[H^+]_w^2}{K_A + [H^+]_w + K_B[H^+]_w^2} \tag{3.5}$$

3.1. Temperature

In the present problem temperature difference also will be examined for silica nanoparticle surface with roughness. Equilibrium constants, ionic diffusivities, and relative permittivity values need to be considered and calculated again according to the varied temperature. In this case relative permittivity of an ionic liquid, equilibrium constants of surface reactions, ionic diffusivities and limiting conductance values of solvated ions are all temperature-dependent. We assume that the liquid phase is a dilute aqueous KCl solution.

$$SiOH \leftrightarrow SiO^- + H^+ \quad K_A = \frac{\Gamma_{SiO^-}[H^+]_w}{\Gamma_{SiOH}} \tag{3.6}$$

$$SiOH + H^+ \leftrightarrow SiOH_2^+ \quad K_B = \frac{\Gamma_{SiOH_2^+}}{\Gamma_{SiOH}[H^+]_w} \tag{3.7}$$
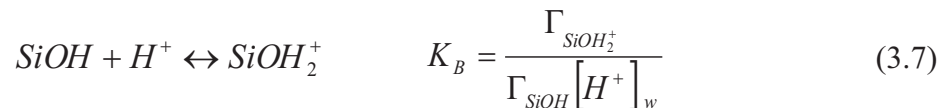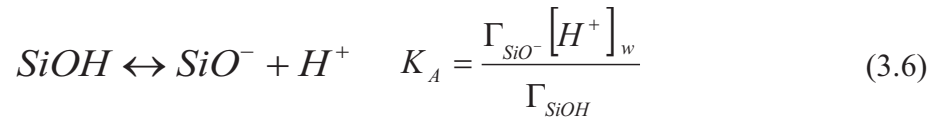
Equilibrium constants of surface reactions on the particle surface will change due to temperature differences. The temperature dependence of equilibrium constants can be calculated using a given formula in (9). Charging behavior of the particle surface is

mostly determined with K_A constant in the pH range between 3 and 9.5 which is used pH range in our study. According to that, the temperature dependence of K_B can be ignored. Proton adsorption on the surface[69] is unlikely to occur in the normal pH range of titration due to the low log K_B values. The charging behavior of the surface is mostly determined by the protonation of surface groups.[70] The temperature dependence of equilibrium constant can be calculated using the Van't Hoff equation (3.8) that contains the temperature and the standard enthalpy change of the reaction. The Van't Hoff equation calculates the variation of the equilibrium constant, K_{eq}, of a chemical reaction when temperature, T, is changing. Here, $\Delta H \ominus$ is the standard enthalpy change for the process.

$$\ln \frac{K(T_2)}{K(T_1)} = \frac{-\Delta_r H^\circ}{R} \left(\frac{1}{T_2} - \frac{1}{T_1} \right)$$
(3.8)

Temperature dependence of K_{eq} can be expressed as:

$$\ln K_{eq} = \frac{-\Delta_r G}{k_B T}$$
(3.9)

$$K_{eq} = \exp^{-\frac{\Delta G^\circ}{k_B T}}$$
(3.10)

$\Delta_r G$ value is the standard Gibbs energy change of the reaction in Equation-1. For the dissociation of H+ on the silica surface $\Delta_r G \cong 13.4\ kcal/mol$ (NaCl). There are several studies which used $\Delta_r G \cong 13.4\ kcal/mol$ value as a standard Gibbs energy change of the reaction. The $\Delta_r G$ for the dissociation of H^+ on the particle surface is 13.4 kcal/mol. The liquid phase is NaCl and SiO_2 particles[71,72]. This value is appropriate when the liquid phase is NaCl, but in our study liquid phase is KCl. According to that $\Delta_r G$ needs to be calculated for our specific case with using current temperature and equilibrium constant value for that temperature range. For T=300 K equilibrium constants are; pK_A=7, K_A=1×10^{-7}, pK_B=1.9, and k_B=0.01258925412. The Equilibrium Constant, K has a straight forward relationship to the Gibbs free energy. Using Equation 3.10 and K_A value that we have for 300 K temperature so we can calculate ΔG° (Gibbs free energy) value for this temperature.

$$\Delta G^{\circ} = -k_B T \ln K \tag{3.11}$$

Using Equation 3.11 and $k_B = 0.0019872041 (\frac{kcal}{mol \times K})$ value $\Delta G^{\circ} = 9.602569 \frac{kcal}{mol}$ is calculated for $T = 300K$. Temperature dependence of Gibbs Free Energy is significant with this given formula in (3.12).

$$\Delta G^0 = \Delta H - T \times \Delta S \tag{3.12}$$

Gibbs free energy value is dependent on temperature difference but for small temperature ranges (298 K – 348 K) $\Delta_r G$ can be considered as constant. Gibbs free energy value that is calculated with using Equation-11 can be used as a $\Delta_r G$ value in our case.

The permittivity of the liquid phase is also temperature-dependent parameter and the relative permittivity of the water can be expressed as where ε_r and ε_0 are the relative permittivity and dielectric constant of a vacuum:

$$\varepsilon = \varepsilon_r \varepsilon_0 \tag{3.13}$$

The temperature dependence of relative permittivity can be expressed as[73–75] ($\Delta T = T - 273.15$):

$$\varepsilon_r(T) = \left[\left(-\left(4.47615 \times 10^6 \right) + \left(4601.28 \times (\Delta T) \right) - \left(2 \times 0.13476 \times (\Delta T)^2 \right) \right) \right] \tag{3.14}$$

This expression used in different studies to calculate the temperature dependence of relative permittivity value. Next, the temperature dependence of ionic diffusivity can be calculated by Nernst-Haskell equation[31,76]:

$$D_j = \frac{RT}{F^2} \left(\frac{\lambda_j^0}{|z_j|} \right) \tag{3.15}$$

where R and λ_j^0 are gas constant and the limiting ionic conductance[54,77] of ionic species j. Limiting ionic conductance (λ_j^0) of ions in aqueous solution shows a strong temperature dependence[77]. Temperature dependency of limiting ionic conductance:

$$\lambda_j^0 = \lambda_j^0 + \alpha_{j1}\Delta T + \alpha_{j2}(\Delta T)^2 + \alpha_{j3}(\Delta T)^3 \tag{3.16}$$

where λ_j^0 is the limiting conductance at temperature T=298.15K. The values for a (a_{j1}), b (a_{j2}) and c (a_{j3}).[78]

Table 3.1. Limiting ionic conductance values at 25°C and values for parameters given in the Equation-16

Ionic Species (j)	λ_j^0 (25°C) (Scm^2mol^{-1})	α_{j1}	$\alpha_{j2}10^2$	$\alpha_{j3}10^4$
H^+	349.85	4.81595	-1.03125	-0.7670
OH^-	199.2	3.52031	0.82700	0.7120
Na^+	50.15	1.09160	0.47150	-0.1150
Cl^-	76.35	1.54037	0.46500	-0.1285

Table 3.2. Limiting ionic conductance values for different ions at 25°C (Haynes, William M. CRC handbook of chemistry and physics CRC press, 2014.)[79]

Cation	λ_+^0 (Scm^2mol^{-1})	Anion	λ_-^0 (Scm^2mol^{-1})
H^+	349.6	OH^-	199.1
Li^+	38.7	F^-	55.4
Na^+	50.10	Cl^-	76.35
K^+	73.50	Br^-	78.1
Rb^+	77.8	I^-	76.8

Table 3.3. Limiting equivalent conductance of cations in water from 0 to 100°C (from Robinson and Stokes, 1968)[80]

Ion	0°C	5°C	15°C	18°C	25°C	35°C	45°C	55°C	100°C
H^+	225	250.1	300.6	315	349.8	397.0	441.4	483.1	634
Li^+	19.4	22.8	30.2	32.8	38.7	48.0	58.0	68.7	156
Na^+	26.5	30.3	39.8	42.8	50.1	61.5	73.7	86.9	151
K^+	40.7	46.8	59.7	63.9	73.5	88.2	103.5	119.3	195
Rb^+	43.9	50.1	63.4	66.5	77.8	92.9	108.6	124.3	-
Cs^+	44	50.0	63.2	67	77.3	92.1	107.5	123.7	-

Table 3.1 shows the limiting ionic conductance values of ionic species at 25°C and parameters which are given in the equation that gives temperature dependency of limiting ionic conductance.[54,78]

In the literature, there is no defined significant equation that gives temperature dependency of limiting ionic conductance of K^+ ion. To accomplish this, we need to define an equation using determined limiting equivalent values experimentally from the literature according to elevated temperatures. Limiting ionic conductance value is calculated as $\lambda_{j(K+)}^0 = 73.50 \ S \times cm^2/mol$ for T=298 K.
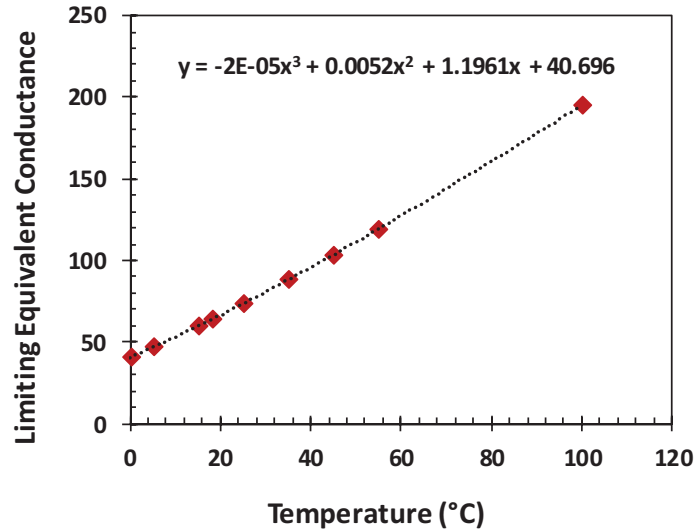
Figure 3.1. Variation of limiting equivalent conductance values of K^+ with temperature

The equation is defined by using experimental data which exists in the literature. These values show the temperature variation of limiting equivalent conductance values of K^+. According to these values polynomial 3rd order equation added on the graph. This equation shows similar behavior with a general equation that gives the temperature variation of limiting ionic conductivity as given in the Equation-16.

This equation gives temperature dependence of limiting ionic conductivities of K^+ is obtained from the given data on the above:

$$\lambda_j^0 = \left(-(2\times10^{-5})\times(\Delta T)^3 + 0.0652\times(\Delta T)^2 + 1.1961\times(\Delta T) + 40.696\right) \qquad (3.17)$$

CHAPTER 4

NUMERICAL MODEL

4.1. Numerical Model

In this section numerical model and geometry of the model will be introduced. In Figure 4.1, Figure 4.1-a shows the schematic representation of the present study and Figure 4.1-b shows the geometrical implementation of rough silica nanoparticle in 2-D. The roughness structure on the nanoparticle surface obtained by defining some equations that show the relation between the diameter of particle and geometrical properties of roughness geometry. These equations are; $Theta(\theta) = 360^{\circ}/n$, $R_R = \tan(\theta) \times R_P$ and $\alpha = 360^{\circ}/2 \times n$ where n is a number of indentations on the particle surface, theta (Θ) is the angle between centers of a recess and protrusion, α is the angle between two protrusions, R_R is the radius of roughness and R_P is the radius of the particle. Using these equations roughness geometry on the particle surface is created.
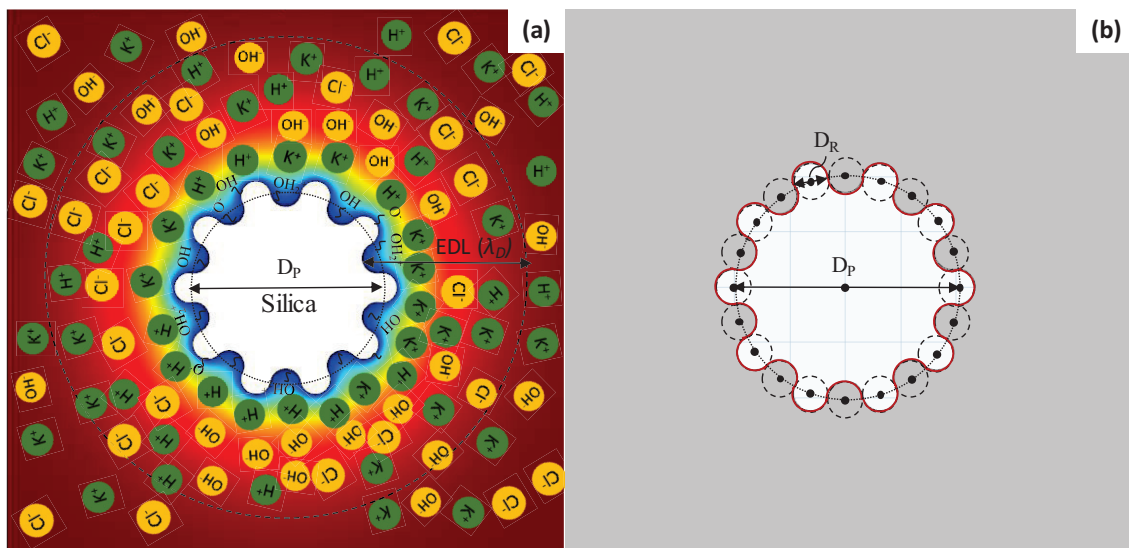

Figure 4.1. (a) Schematic representation of the numerical model. (b) Representation of geometrical structure of rough nanoparticle

Silica nanoparticle with roughness structure on its surface considered as immersed in an ionized liquid. The liquid phase is made of KCl with the bulk concentration of C_{KCl} and the pH of the electrolyte solution is adjusted by KOH and HCl. There are four ionic species (i.e., N = 4, H^+, OH^-, K^+, and Cl^- dissolved in the solution.

Ci0 is the bulk molar concentration of the ith ionic species and C_{i0} of each species satisfies the electroneutrality condition:

$$C_{10} = 10^{-pH+3} \quad C_{40} = 10^{-(14-pH)+3} \qquad (\text{pH}<7) \qquad (4.1)$$

$$C_{20} = C_{KCl} \qquad C_{30} = C_{KCl} + C_{10} - C_{40}$$

$$C_{20} = C_{KCl} - C_{10} + C_{40} \quad C_{30} = C_{KCl} \qquad (\text{pH}>7) \qquad (4.2)$$

The surface charge density of nanoparticle is modeled by the multi-ion charge regulation model.[26] Poisson equation gives electric potential distribution and the Nernst-Planck equation gives ionic mass transport. These two governing equations solved together using the charge regulation model as a boundary condition on a nanoparticle surface. The surface charge density of a nanoparticle surface is calculated by using this equation:

$$\sigma_w = -\frac{F\Gamma_{total}}{N_A} \frac{K_A - K_B\left[H^+\right]_w^2}{K_A + \left[H^+\right]_w + K_B\left[H^+\right]_w^2} \qquad (4.3)$$

The hydrogen concentration in Equation 4.1 is updated in each cycle according to the numerically solved results and used as input for the next iteration; thereby, the ionic concentration and electrical potential are solved simultaneously. The surface charge depends on the bulk concentrations of the ions, which are based on the pH of the ionic solution and the salt concentration of the solution. By using this iterative procedure surface charge density of rough nanoparticles can be obtained.

4.2. Computational Details

As stated previously, computations were carried out using boundary conditions. PNP equations in 2-D Cartesian coordinates solved numerically using COMSOL Multiphysics software and during the solution of governing equations, the Finite Element Method was employed. The number, distribution, and shape of the computational elements are crucial when using the finite element method. Optimum mesh case was selected by performing mesh independency tests. Different mesh densities were selected and the mesh dependency of the results was compared. Finer mesh adopted a close region to the EDL and surface of the nanoparticle. Physical parameters used in the simulations are; $\varepsilon_0 \varepsilon_f = 7.08 \times 10^{-10} F/m$, $R = 8.31 J/(mol \times K)$, $F = 96490 C/mol$, $T = 300K$, $N_{total} = 8 sites/nm^2$ $pK_A = -\log K_A = 7$ and $pK_B = -\log K_B = 1.9$.

To validate the current model simulations were done at proper conditions (C=50 mM, Dp=9 nm, pK_A=7.2, pK_B=1.9, N_{total}=4.75mol/m² [81]) and compared with experimental data which exists in the literature[82]. As seen in Figure 4.2 experimental data and numerical data show an agreement.
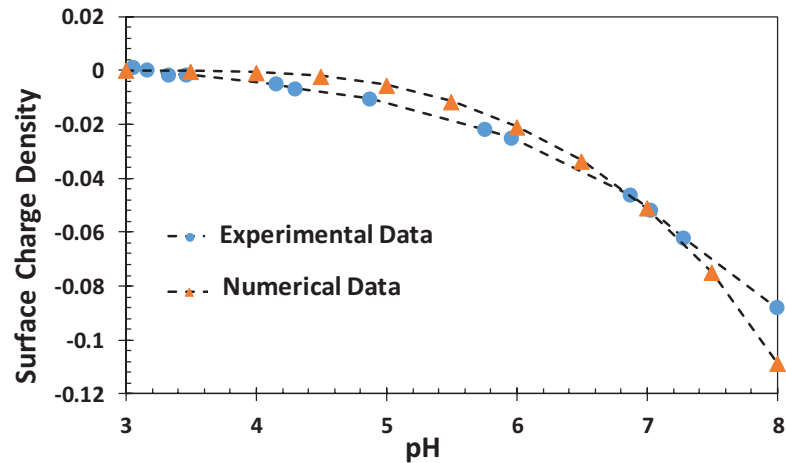
Figure 4.2. Comparison between numerical and experimental data

Temperature model is validated by numerical simulations which are performed at proper conditions (pH=5,7,9, N_{total}= $5 \times 10^{-7} \, mol/m^2$, $\Delta G° = 13.4 \, kcal/mol$, $C_{NaCl} = 10^{-3} M$, $pK_B = 2$, $pK_A = 7$). To validate the given numerical procedure present problem

solved by COMSOL Multiphysics software using the finite element method. We assume that the liquid phase is NaCl as in the previous study that we choose for verification and pH is adjusted by NaOH and HCl. We modeled silica nanoparticle with a flat surface, at given dimensions (R=20 nm) immersed in an electrolyte solution (NaCl). Obtained numerical data compared with surface potential values which were given in the previous study[31].

As shown in the figure our numerical data shows good agreement with numerical values obtained from the previous study that we used for verification.

Figure 4.3. Comparison of the surface electric potentials that calculated with our temperature model (markers and dotted line) and calculated numerical data (markers) obtained from previous study[31]

CHAPTER 5

RESULTS

5.1. Roughness Effect

This section aims to investigate surface charge properties of rough silica nanoparticles and how these properties are changing with different particle and roughness diameters. The concentration and pH of the electrolyte solution are kept constant at C=1mM an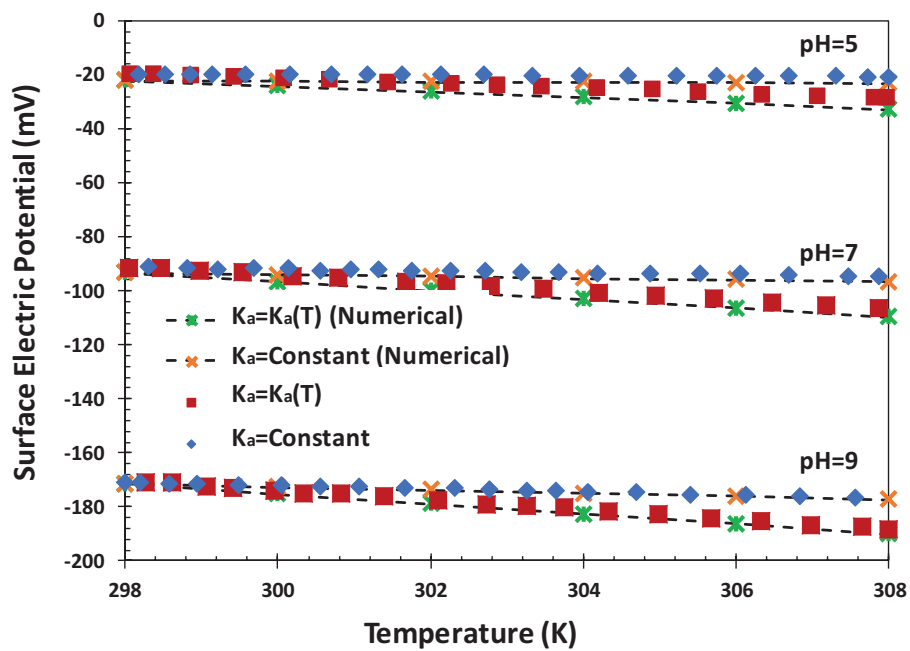d pH=7. Figure 5.1 represents the electric potential contour plots of rough silica nanoparticles according to varying particle and roughness diameters.

As can be seen in Figure 5.1, from bottom to top when roughness diameter is decreasing the gap between the roughness geometries is getting smaller than the EDL thickness. As a result of that formation, electric double layers extending from opposite surfaces will overlap and ionic distribution will change locally. In contrast, when the roughness diameter is increasing EDL overlap effect will be diminished and EDL structure will cover the surface of the rough nanoparticle along the surface. Figure 5.1 shows that from left to right when the particle diameter is increasing curvature effect will occur on a nanoparticle surface. The curvature effect is formed when the surface to volume ratio is decreasing. These two main effects (EDL overlap and curvature) can be seen on rough nanoparticle surface and their interactions with other surfaces. As a result of these effects, ionic distribution and surface charge properties will change locally on the nanoparticle surface. Ionic distribution and electric potential distribution will change depending on roughness and particle diameter. EDL overlap at the beginning started on the bottom region of roughness geometry than with a decreasing diameter EDL overlap will expand to the top region of the geometry.

Next, surface charge distributions need to be measured locally and investigated more detailed. So, surface charge densities calculated locally on rough nanoparticle surface according to local ionic concentration. Figure 5.2 shows surface charge density distributions on the rough nanoparticle surfaces as given in Figure 5.1 which is calculated through along the normalized radial position ($x/\pi D_R$).
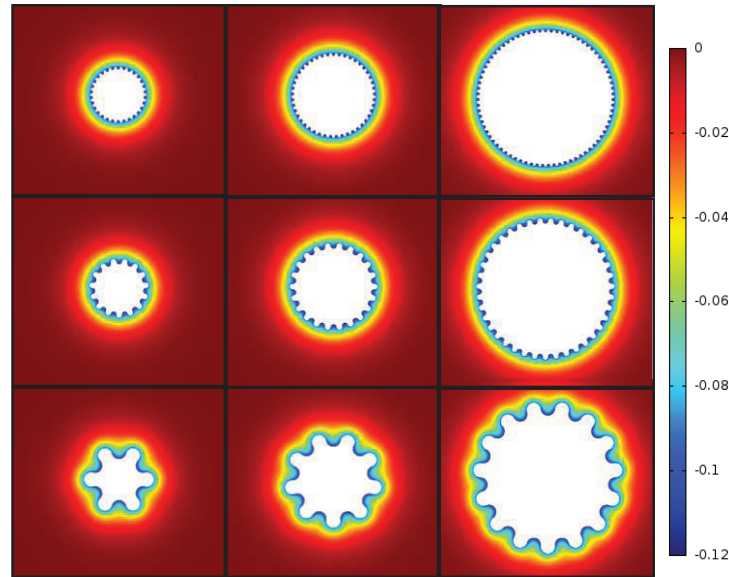
Figure 5.1. Electric potential distributions of different particle diameters and roughness diameters at pH=7 and C=1mM. The particle diameter is increasing from left to right when roughness diameter is constant, roughness diameter is increasing from bottom to top when the particle diameter is constant (D_P=40nm, 60nm, 100nm D_R=2nm, 4nm, 10nm)

Also, the average surface charge density of rough nanoparticle, flat nanoparticle, and flat plate added on the graph for a detailed comparison. Electrolyte solution concentration is constant at 1 mM and the same for each case. Also, the pH value is kept constant at 7. As can be seen in the figure with increasing roughness diameter (from a to g) average surface charge is becoming similar to the predictions of the flat surface theory because the EDL overlap effect shows diminishing behavior with higher D_R values. In contrast to that, when roughness diameter is decreasing EDL overlap and curvature effect become more dominated and surface charge value of rough nanoparticle surface differs from the flat surface calculations. When the particle diameter is decreasing the average surface charge density is increasing due to the curvature effect. The average surface charge density is increasing with a decreased diameter due to the curvature effect. In contrast, EDL overlap decreasing the average surface charge density and the average surface charge density becomes lower than the surface charge value of a flat surface. For instance, we can see from the figure (from a to c) that with an increased particle diameter surface charge value of a flat particle is decreasing and getting closer to the flat surface theory for 100 nm nanoparticle. Because with an increasing particle diameter curvature effect will be decreased and surface charge density will be affected by this variation. In this case, roughness diameter is smaller (2nm) and due to that EDL overlap effect also

dominated. Also with an increasing roughness diameter (from a to g) when the particle diameter is constant average surface charge is becoming increasingly and getting similar with predictions of the flat surface theory. In this chosen case particle diameter is smaller (40nm) and shows there is a difference between flat particle surface charge and flat surface theory due to the increased curvature effect.
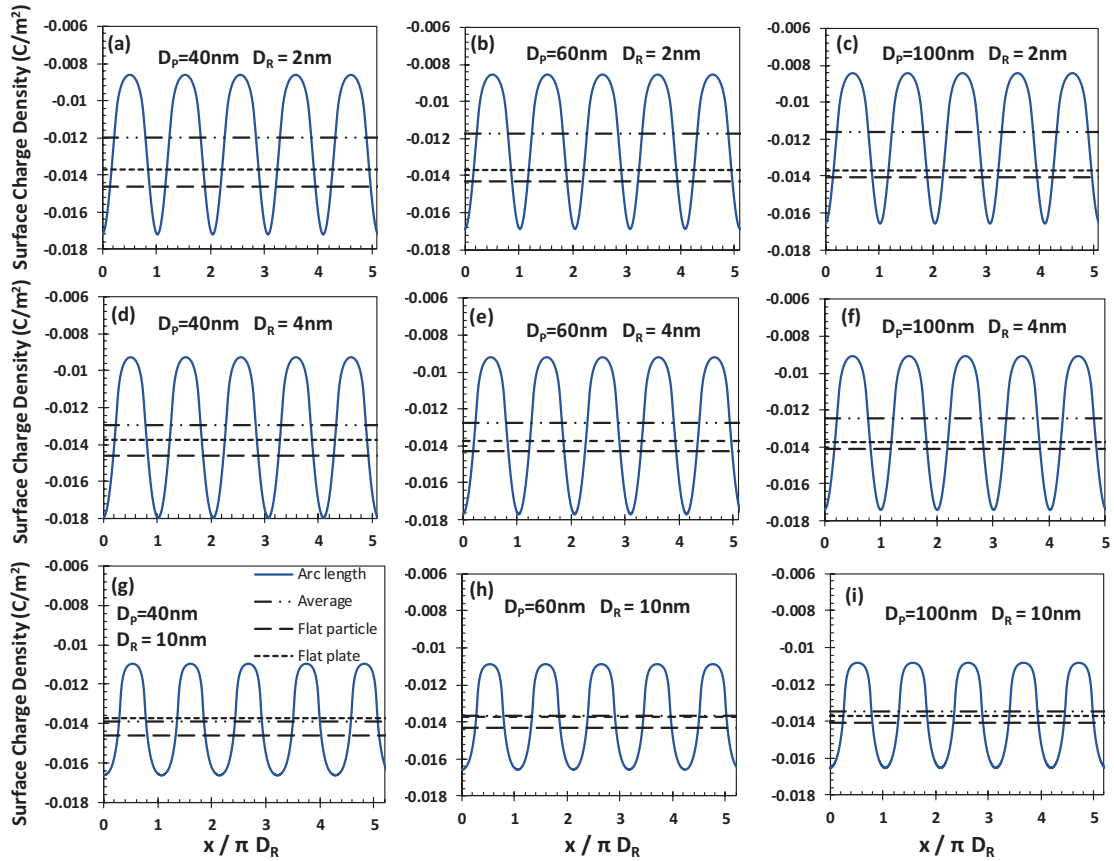
Figure 5.2. Surface charge density distribution on rough silica nanoparticle with different varying particle and roughness diameters (at pH=7, C=1mM). a-d-g, b-e-h, and c-f-i cases have 40nm, 60nm and 100nm particle diameters, while a-b-c, d-e-f and g-h-I cases have 2nm, 4nm, 10nm roughness diameters.

Figure 5.3 shows the surface charge density values measured at the top and bottom regions of roughness geometry. This graph represents the local variation of surface charge densities. Measured surface charge density values normalized with flat plate theory. This characterization was used because the impact of particle diameter can be clearly seen. The upper graph shows the variation of the normalized surface charge density values with respect to different roughness diameters. The flat particle line on this graph represents the

flat particle surface charge values of nanoparticles which has a diameter at given roughness diameters. Flat particle surface charge values are showing decreased behavior with an increasing roughness diameter because of the curvature effect. We can see that the surface charge densities will be getting closer to the flat particle surface charge density and showing similar behavior with an increasing diameter of roughness. Also, we can observe that from the Figure 5.3-a, surface charge density values measured on the top region of the roughness geometry first increased with an increasing roughness diameter, then reached a peak value at a certain diameter. After that with increasing diameter of roughness top surface charge density shows decreasing behavior and reached flat particle value. Figure 5.3-b shows the surface charge density distributions that are calculated in the bottom region of the roughness geometry according to different roughness diameters. Bottom surface charge values are decreasing at the beginning with an increasing roughness diameter than reached at a peak value at a certain diameter. When roughness diameter continues to increase, surface charge densities will show an increasing behavior and reaches a flat particle surface charge density.

Figure 5.4 shows a comparison of flat surface charge density, average surface charge density on rough nanoparticle and surface charge densities which are calculated on the top and bottom region of roughness geometry according to different particle diameters. From left to right particle, the diameter is increasing (a) 40nm, b) 60nm, c) 100nm). We can see from the graph for 100 nm when roughness diameter reaches a certain value, the surface charge measured at top of the roughness and the average surface charge will get closer to normalized flat particle value. In contrast to that surface charge density values calculated on the bottom of the roughness will stabilize eventually but can't reach the flat surface theory. This behavior can be seen due to the overlap effect formed in the bottom region of roughness geometry. We can see that this overlap effect is more effective when the roughness diameter is smaller than the EDL thickness. Surface charge densities at the top of the roughness geometry are higher than flat particle surface charge. At the beginning surface, charge density values are increasing but then begin to decrease with an increased roughness diameter. Surface charge densities at the bottom show an opposite behavior and they are lower than the flat particle surface charge values. At the bottom surface charge densities show an increasing behavior with an increased diameter.
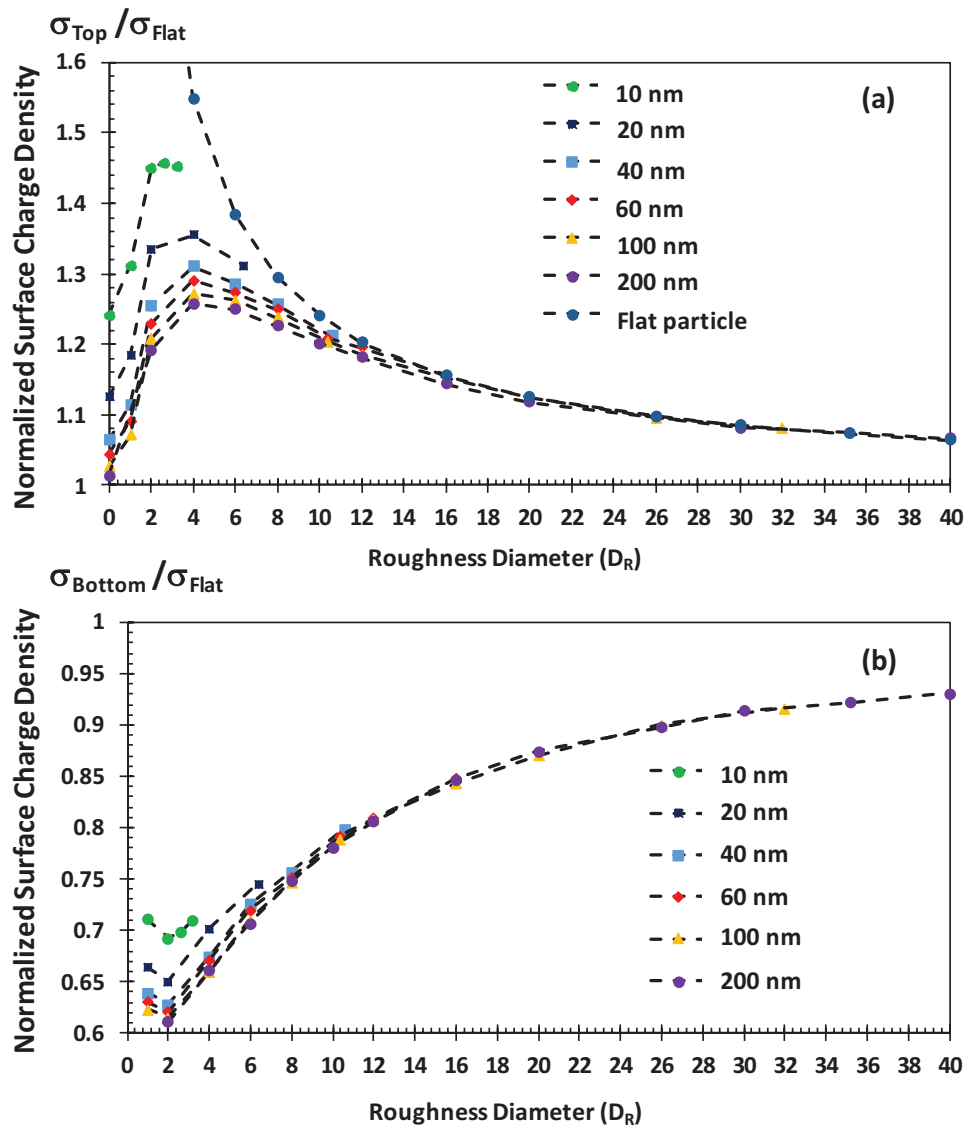
Figure 5.3. Normalized surface charge density distributions measured from top and bottom region of rough nanoparticles and their variation according to the different roughness and particle diameters (C=1 mM, pH=7)

Surface charge variation on the top of the roughness geometry shows a similar behavior with a single particle. Average and top surface charge densities will be reached to flat particle surface charge with an increased diameter. Because, in this case on the top of the roughness structure curvature and EDL overlap effect has been observed. But on the bottom region, we can also see the EDL overlap effect. This effect can change the ionic distribution and surface charge variation in the bottom region.
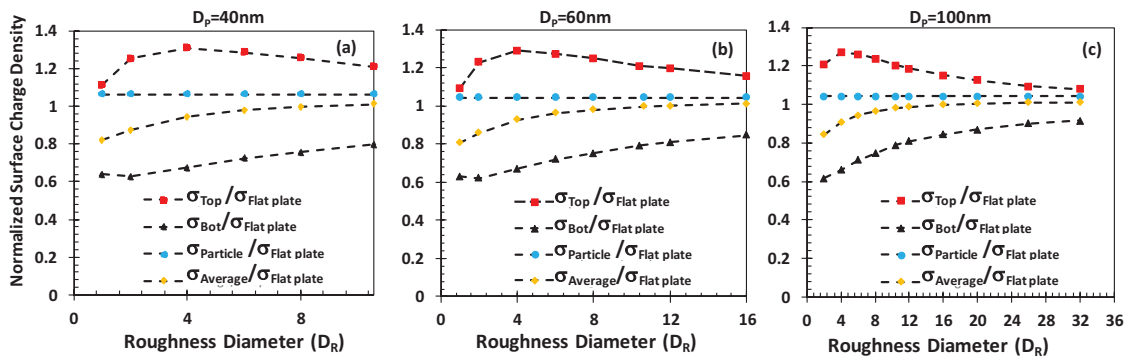
Figure 5.4. Normalized surface charge densities measured from the top and bottom regions and comparison of them between flat particle and average surface charge density values (Particle diameter is increasing from left to right D_P=40nm, 60nm, 100nm, C=1mM, pH=7)

Since we examined surface charge variation locally and showed a comparison between local values and average values. As the next step in Figure 5.5, we gather and show all surface charge variations according to different particle and roughness in this graph. Figure 5.5 shows the variation of the normalized surface charge density values with different particle and roughness diameters. With an increasing particle and roughness diameters, surface charge values will reach the flat surface theory. This behavior occurs due to the decreased surface to volume ratios. These surface charge density values are average values which are measured on a rough nanoparticle surface and normalized with flat surface predictions. All lines on the graph show an increasing behavior and reached a flat surface prediction at a certain diameter. Then they will be fixed at flat surface values. Also, in the bottom graph below, electric potential distributions is plotted according to variation of roughness diameter. Electric potential distributions will change with varying roughness diameter. For instance, smaller roughness diameters EDL structure will expand through the roughness geometry and will overlap. But for higher diameters, EDL thickness is getting smaller than the roughness diameter and will cover the rough surface along the arc length path.

In Figure 5.6, surface charge variation examined according to different particle and roughness diameters and pH variation also added and examined. The concentration of the electrolyte solution kept constant at 1mM. For each graph particle diameter is constant (a) 40 nm, b) 60 nm, c) 100 nm), roughness diameter and pH values are varied. Similar behavior as seen in the previous figures was also observed in this figure.
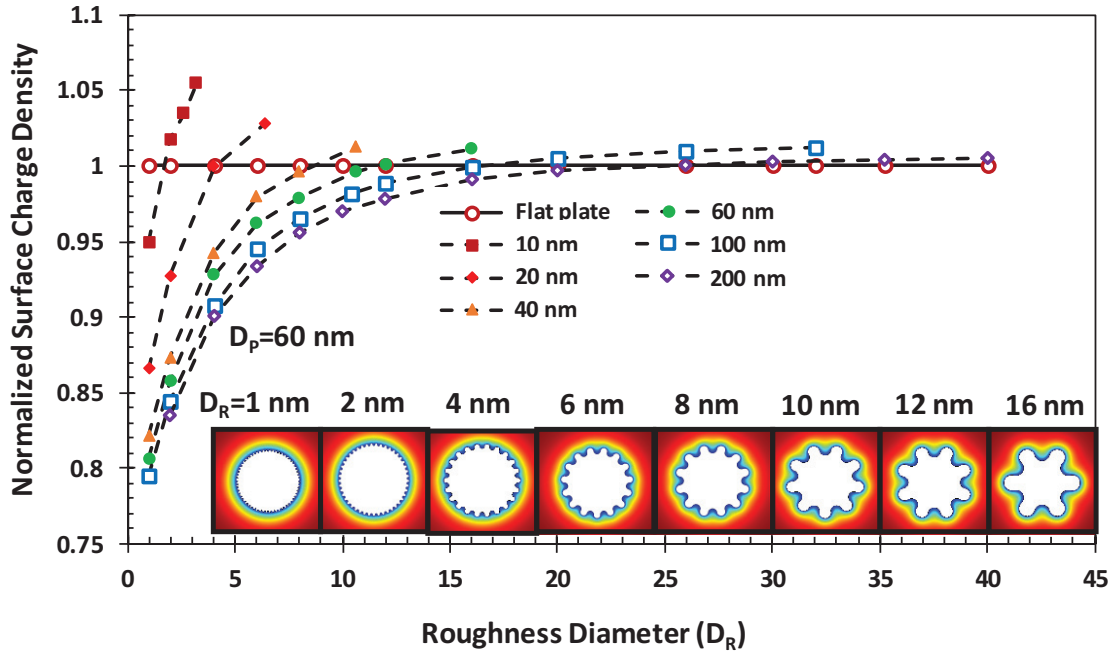
Figure 5.5. Average surface charge densities measured along the arc length line (normalized with flat surface theory) and their variance with varying roughness and particle diameter. (C=1 mM, pH=7)

With an increased roughness diameter surface charge values getting closer to flat surface theory predictions. This is due to the EDL overlap on the bottom region diminished and curvature effect becomes dominant on the surface of the rough nanoparticle. With an increased pH surface charge variation decreased at the beginning and then reached a peak value at a certain pH value. This certain pH value is different for each roughness diameter. This value is getting smaller with an increasing roughness diameter. For instance, in Figure 5.6-a which represents the surface charge variation of a nanoparticle with 40 nm diameter, when roughness diameter is 10 nm that is the highest roughness diameter in this specific case the peak pH value seems around at 4.5. Also for 4 nm roughness diameter, the peak value seems around at 5.5. After surface charge density reaches the peak value, it begins to show decreasing behavior. Thus, we expect that it will reach a flat surface prediction and fixed that constant value. We can see this expected behavior clearly with higher roughness diameters for each of the three cases. In contrast, it was not observed for smaller roughness diameters because for smaller roughness diameters EDL overlaps more dominated and affected the ionic distribution and surface charge density. We can observe that the pH variation also has an impact on the surface charge density distribution. This behavior occurs due when the pH level is

34

increasing, the bulk concentration of H^+ ions decreases. For this reason, H^+ concentration on the rough nanoparticle surface results in a lower concentration. Surface charge density will have higher values due to the difference in ionic concentration on the surface.
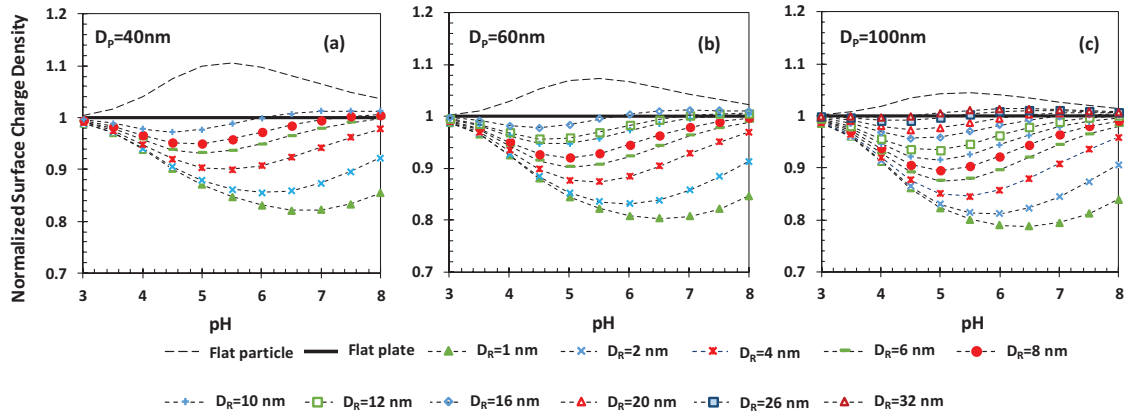

Figure 5.6. Comparison of the surface charge density values of the flat particle, flat surface and rough nanoparticles with different roughness diameters according to the different pH. (Each graph has constant particle diameter and changing from left to right $D_P=40nm$, 60nm, 100nm, and C=1 mM, pH=7)

In Figure 5.7, normalized surface charge densities variation with pH is examined according to different roughness diameters. As shown, we observed a complex behavior and no clear explanation could be established about pH effect on the surface charge distribution. We see that some cases show similar trends and form groups among themselves but there is not a clear relationship between these cases. We can deduce that using only roughness diameter as a characterization parameter is not enough. Because two main effects are important for charging behavior that occurs on the rough nanoparticle surface. These are curvature effects which are observed due to the increased particle diameter and electric double layer overlap which occurs when opposite surfaces are closer than the electric double layer thickness. Accordingly, D_P and λ (EDL thickness) need to be implemented with D_R as a characterization parameter.

In Figure 5.8, surface charge density that is measured on a rough nanoparticle surface along the arc length path normalized with flat surface values. Also, different characterization is used such as the diameter of roughness is divided by the diameter of particle (D_R/D_P). This type of characterization is needed for investigating the effect of roughness diameter.
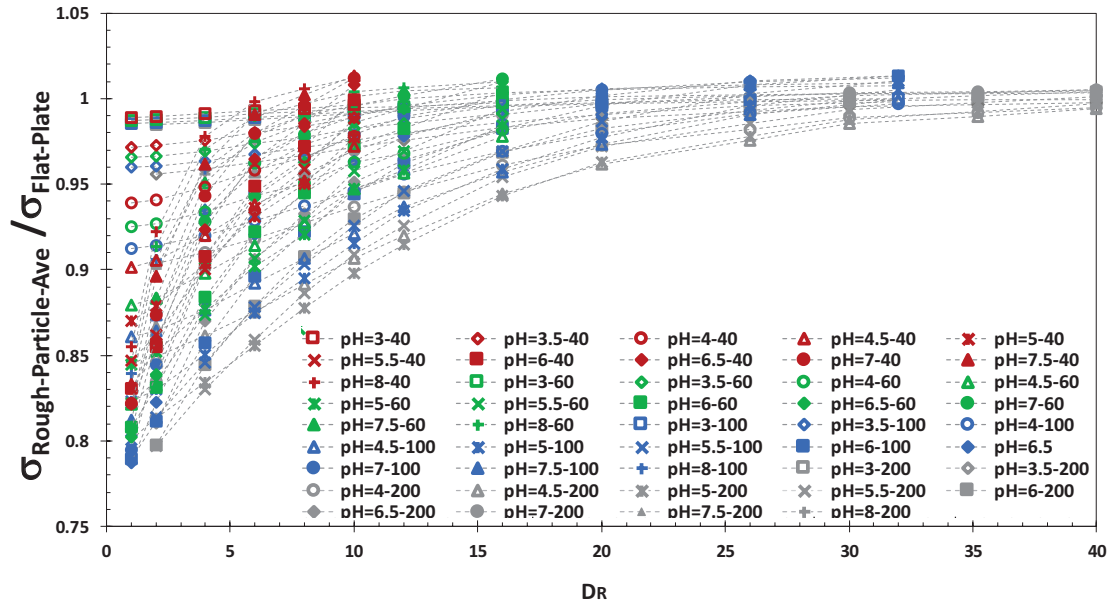
Figure 5.7. Normalized surface charge densities (arc length) for different pH and diameters and their characterization according to the change of D_R

Each color of the marker represents different particle diameters such as 40 nm, 60 nm, 100 nm, 200 nm, and different marker geometries represent the varying pH levels 3 to 8. For smaller D_R/D_P values which means smaller roughness diameters surface charge densities show strong variation according to different pH levels. When roughness diameter is increasing this strong variation will change and surface charge densities show more stable behavior and will be fixed at near 1. The graph shows that pH variation is more effective in cases with smaller roughness diameter. This behavior can be seen due to the EDL overlap effect. EDL overlap is more dominant for smaller roughness diameters and also pH variation will change ionic distribution and surface charge property. Also for smaller D_R/D_P values these varying surface charge densities show similar behaviors and have similar values in some cases. For example, at lower pH levels (pH=3, 3.5, 4) the behavior of the variance seems stabilized and fixed at certain values for different particle diameters. But, when the pH level is increasing (pH=4.5, 5 ...) surface charge variation starts to decrease. In contrast, for higher D_R/D_P values, surface charge density variation is not very significant and only shows differences slightly for different pH levels.

As a next step, λ (EDL thickness) is added to the characterization parameter. In Figure 5.9, normalized surface charge distributions are investigated with different pH levels according to different particle and roughness diameters.
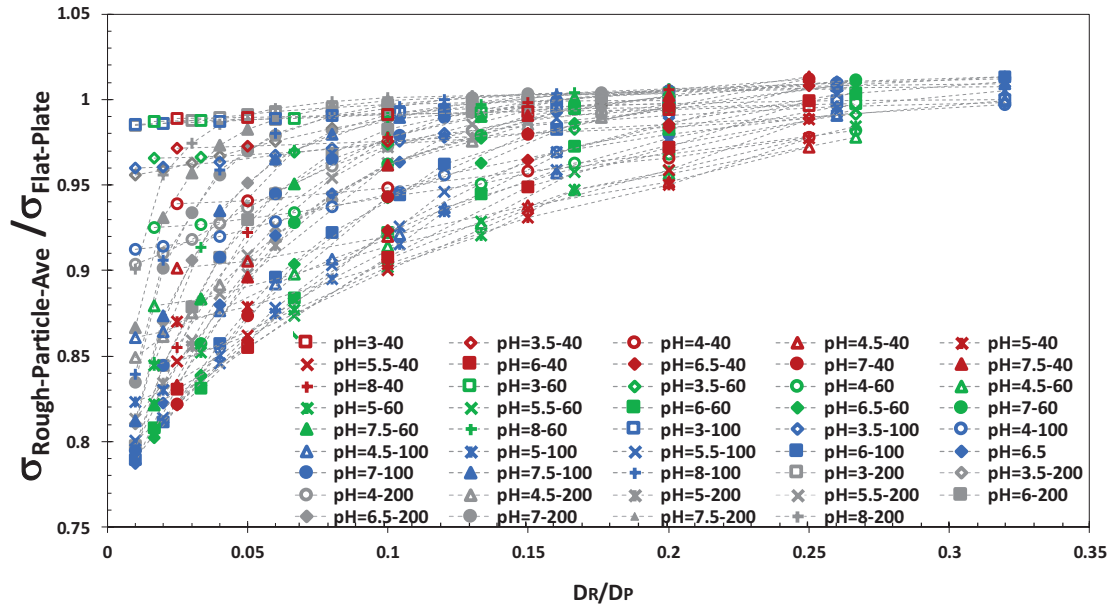
Figure 5.8. Normalized surface charge densities (Arc length) for different pH and diameters and their variation according to the characterization of D_R/D_P

Variation of normalized surface charge distributions is investigated using $(D_R/D_P) \times (D_R/\lambda)$ as a characterization parameter. Using this characterization parameter effect of particle and roughness diameter and electric double layer thickness are examined and these are effective in the formation of nanoparticle surface charge.

As shown in the graph, for all pH levels normalized surface charge distributions reached to theory with an increasing characterization parameter $(D_R/D_P) \times (D_R/\lambda)$. However, when the characterization parameter $(D_R/D_P) \times (D_R/\lambda)$ is decreasing surface charge variation behavior is becoming a more complicated and similar trend is observed with previous graphs. Three different characterization parameters are used but surface charge variation behavior according to pH cannot be observed clearly. There are some specific cases formed groups and showed similar behaviors but there is not a proper relationship that can be determined between them.

In Figure 5.10, the normalized surface charge variations according to $(D_R/D_P) \times (D_R/\lambda)$ parameter showed in different graphs for each pH level. Each graph shows normalized surface charge distributions for different particle and roughness diameters according to $(D_R/D_P) \times (D_R/\lambda)$ parameter at a specific pH level. Thus, surface charging behavior can be seen more clearly for each pH level.
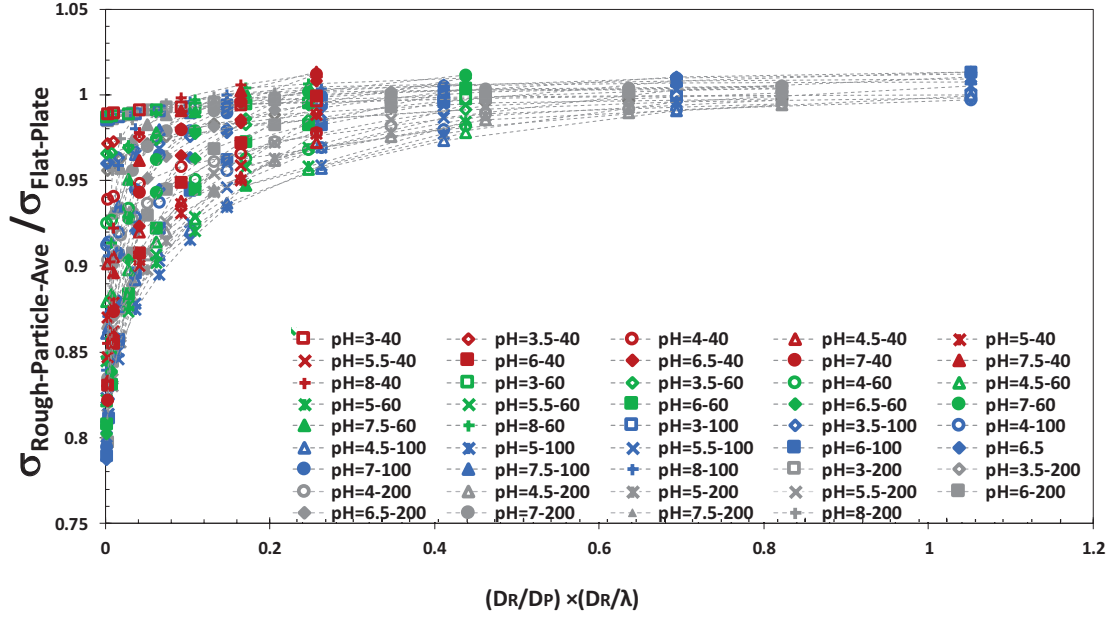
Figure 5.9. Normalized surface charge densities (Arc length) for different pH and diameters and their variation according to the characterization of $(D_R/D_P) \times (D_R/\lambda)$

In Figure 5.11, the surface charge distributions calculated for all particle and roughness diameters and normalized with theory subtracted from 1 were summed for each pH level. Then, graphs were created showing the variation of surface charge distributions for each pH value according to $(D_R/D_P) \times (D_R/\lambda)$ parameter.

Surface charge density variation is examined in detail in previous graphs but there is not a proper explanation observed about pH effect. In order to do that, there is an equation given below :

$$\frac{\sigma_{Rough-Particle-Ave}}{\sigma_{Flat-Plate}} = 1 - Ae^{-B\left(\frac{D_R^2}{D_P \times \lambda}\right)} \quad (5.1)$$

Here, the values obtained by subtracting the surface charge distribution values normalized according to the theory from 1, and obtained values are defined by an equation in the form $-Ae^{-Bx}$.

Using this equation, A and B values for each pH were calculated and surface charge behavior was shown in the graphs. For characterization, the parameter $(D_R/D_P) \times (D_R/\lambda)$ was used for the x-axis and placed in the equation. The reason for selecting this parameter is to ensure that the effect of the thickness of the EDL can be

examined due to the overlap of the EDL's as well as the particle and roughness diameter effects.
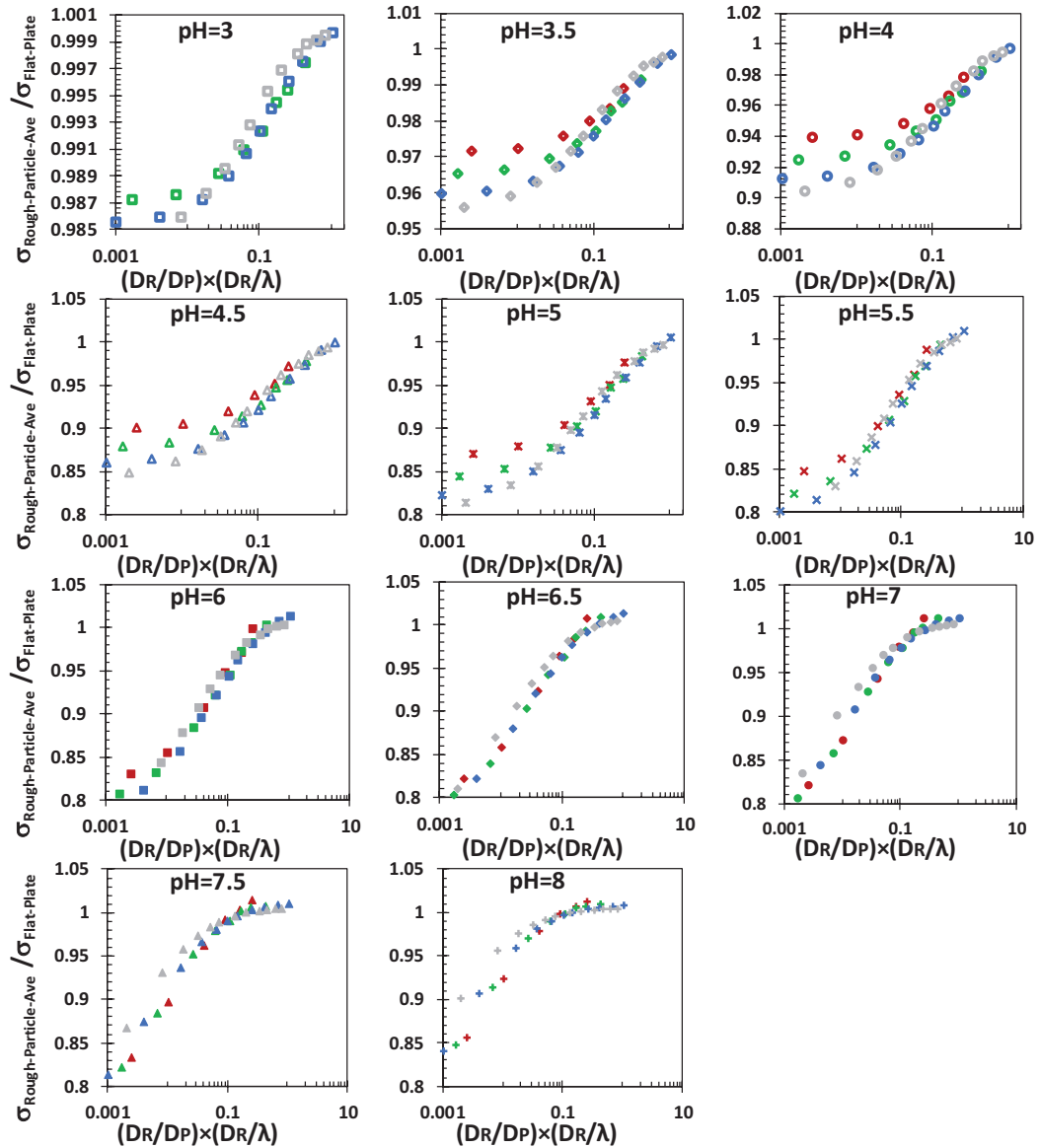
Figure 5.10. Normalized surface charge distributions for each pH level and different particle and roughness diameters

After that, the trend lines showing the behavior tendency of the surface charge distributions relative to the pH on the data seen in the graph created for each pH value were defined by an exponential function and phenomenological fit was created. A and B

values were calculated for each pH value using the exponential function equation which defines trend lines.
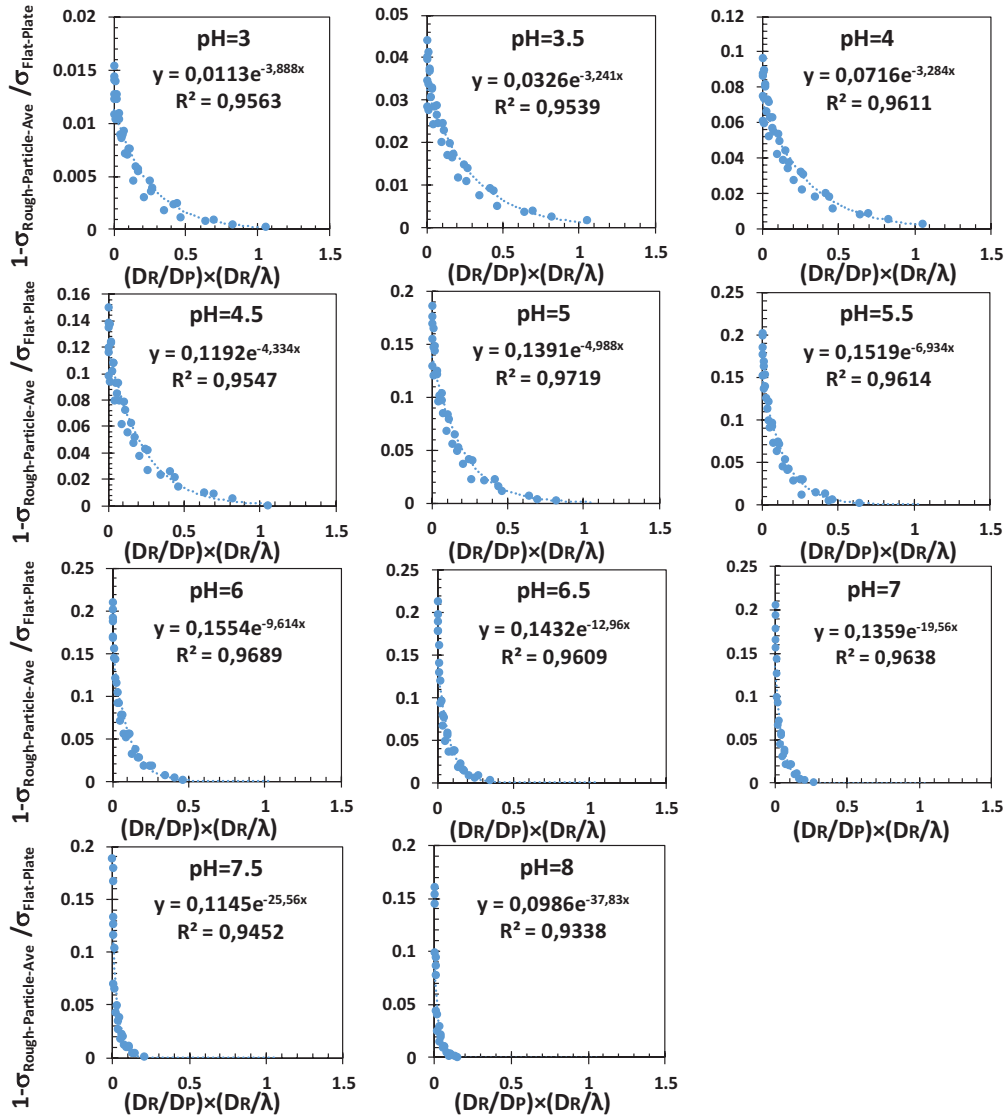
Figure 5.11. Phenomenological fit showing the variation of the surface charge distributions normalized with theory according to $(D_R/D_P)\times(D_R/\lambda)$ parameter for different pH's

Next, graphs showing the variation of A and B values according to different pH levels were created. In Figure 5.12, graphs were created for the pH-related variation of A and B values calculated for each pH value. Trend lines showing the pH-dependent behavior of A and B values for each pH value of the equation defined in the form of $-Ae^{-Bx}$ are defined by a third-order and fourth-order polynomial equation. In this way,

a general equation was defined which shows the distribution behavior of surface charge distributions normalized with theory taken from a difference of 1 for given pH value. A model was created in the form of $\dfrac{\sigma_{Rough-Particle-Ave}}{\sigma_{Flat-Plate}} = 1 - Ae^{-B\left(\dfrac{D_R^2}{D_P \times \lambda}\right)}$ showing the pH-dependent surface charge distribution of a surface of a rough nanoparticle.

$$A = 0,0017\,pH^4 - 0,0369\,pH^3 + 0,2789\,pH^2 - 0,8132\,pH + 0,7988 \tag{5.2}$$

$$B = 0,4089\,pH^3 - 4,5497\,pH^2 + 17,116\,pH - 18,01 \tag{5.3}$$
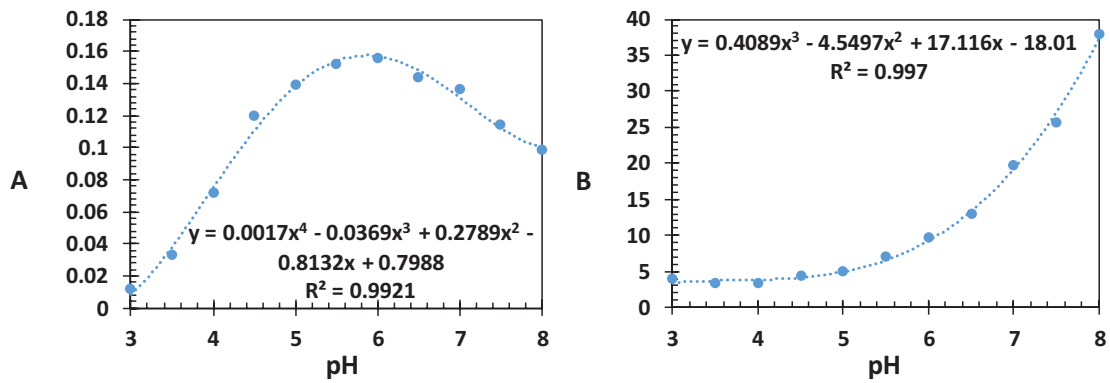
Figure 5.12. A and B values calculated according to different pH levels.

After that, surface charge distributions were calculated using the defined model and equations that show pH dependence of surface charge behavior of rough nanoparticle. Then, the relative error is calculated using calculated surface charge distributions with the empirical model and surface charge values calculated numerically for each pH level in Figure 5.13.

Further investigation is carried out to determine electrostatic behavior inside roughness cavities. To accomplish that, circular arcs are defined in cavities and fictitious surface charges are measured on the arcs which are parametrized with the angle θ. Arcs are shown in Figure 5.14 for varying θ values. Theta (θ) is measured from the center of

roughness diameter and defines the point in which tangent to roughness diameter in order to measure fictitious surface charge.
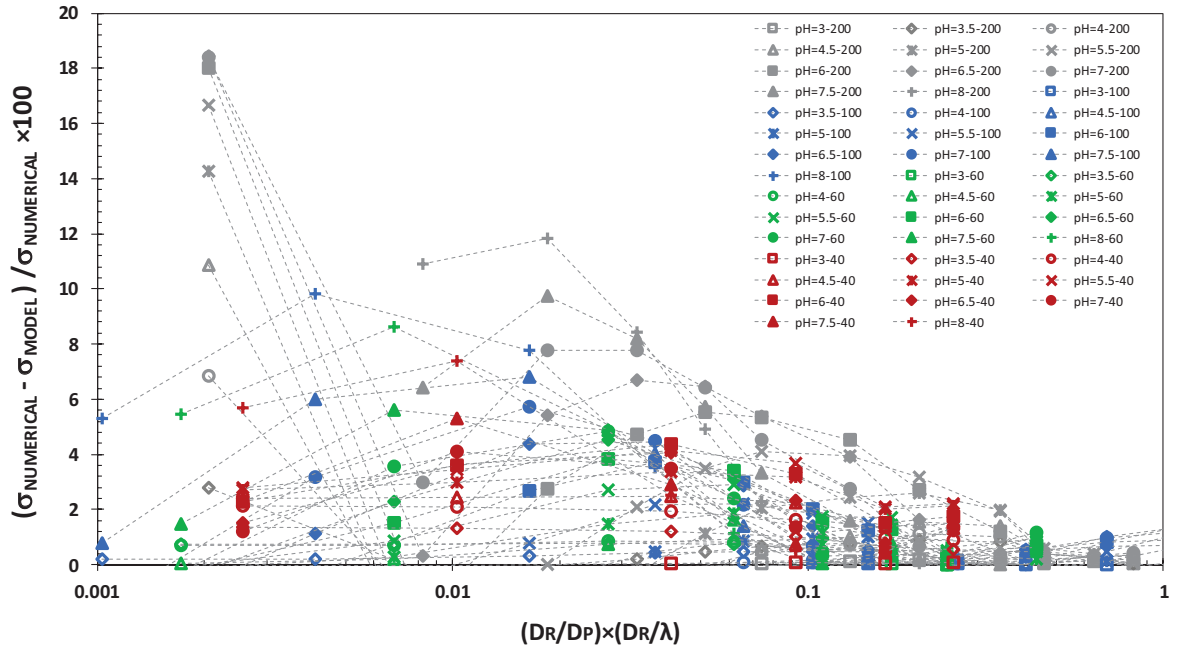
Figure 5.13. Determined relative error values of surface charge densities between that determined with an empirical model and numerically calculated at different roughness and particle diameters and pH

In Figure 5.14b, θ vs normalized roughness diameter is shown. Roughness diameter is normalized with a molecular thickness (0.3 nm). Roughness diameter in Figure 5.14b expresses the diameter of a nanoparticle that has the same surface charge on the arcs. Red filled circles on Figure 5.14b show phenomenological fit and the general trend can be expressed in the form of $90 \times e^{-ax}$.

In Figure 5.15, a detailed investigation of surface charges on tangential arcs for three different particle diameters is shown. Normalized surface charge is expressed as a function of roughness diameter for varying θ values. The surface charge of the rough nanoparticle is presented in the θ=0 case. As θ increases divergence normalized surface charge increases. Polynomial functions are fitted to each θ value to predict behavior at small roughness diameters also interaction boundary is introduced. For a relatively large roughness values interaction boundary assumed to be surface charge density on the interface. However, as roughness diameter decreases, it is the fact that there is no apparent

interaction between roughness and the environment. Therefore, interaction boundary extrapolated to the case that there is no divergence for zero roughness diameter.

Figure 5.14. Schematic representation of the circular tangential arcs of the particle interactions with its environment by varying interaction angle Theta (θ)

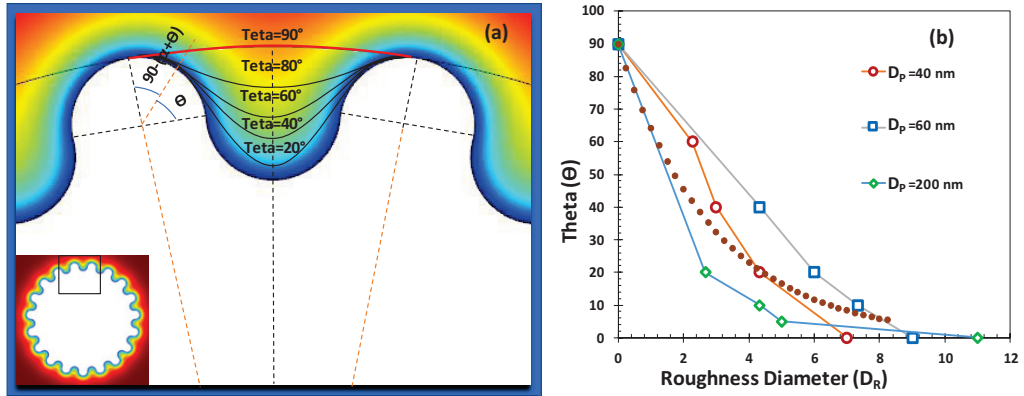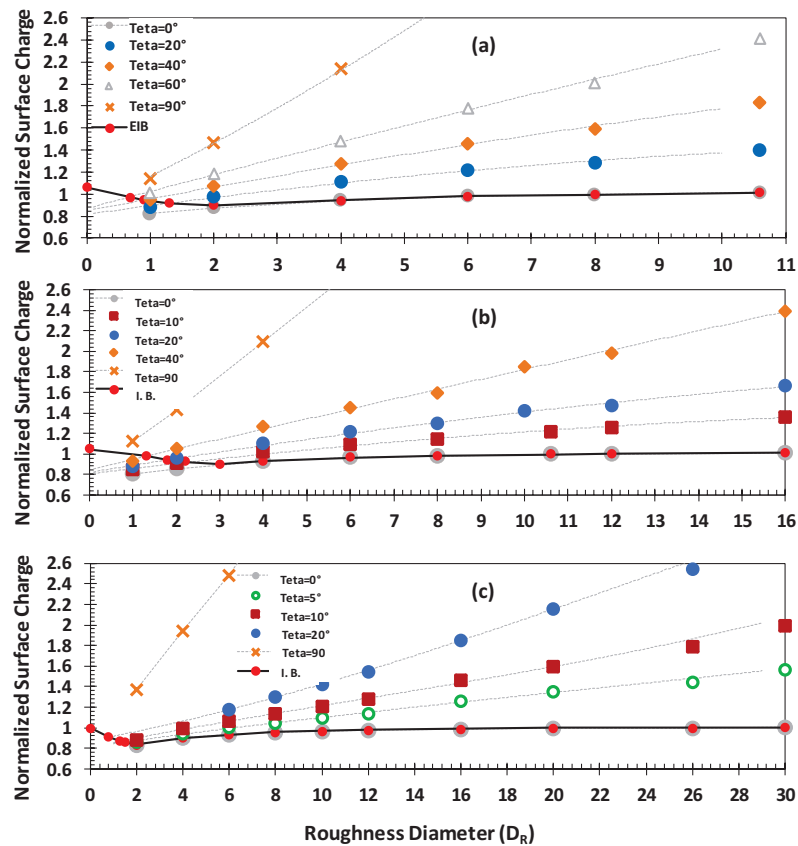Figure 5.15. Normalized surface charges that are measured on circular arc lengths with varying Theta (Ө) angles (40 nm, 60nm, 200nm)

5.2. Temperature Effect

The aim of this section is to investigate the temperature effect on the surface charging of rough silica nanoparticles. Figure 5.16 shows the electric potential distribution on a rough nanoparticle surface at different temperatures. Each column has the same particle diameter and temperature value and each row have the same particle and roughness diameter. From left to right temperature shows a variation (298, 313, 323 K) and from top to bottom roughness diameter is increasing. For the first case, the particle diameter is chosen at 100 nm because the curvature effect intended to be diminished that is occurred due to the decreased particle diameter. In the first case, roughness and temperature, the effect can be observed on the surface of the nanoparticle. For the second case, the particle diameter is at 40 nm and the curvature effect can also be observed at Figure 5.16. Temperature variation will change relative permittivity, ionic mobilities and equilibrium constants of protonation/deprotonation reactions that are occurring on the surface of the nanoparticle.

Figure 5.16. Electric potential contour plots according to different temperature values and different nanoparticle and roughness dimensions (D_P=100 nm, T=298, 313, 323 K; D_R=2, 6, 10 nm; D_P=40 nm, T=298, 313, 323 K, D_R=2, 6, 10 nm)

When the temperature is increasing ionic mobilities also show an increasing behavior[31]. This behavior is consistent with an experimental study from the literature[31,83].

With increased ionic mobilities ionic distribution on the surface will change and electric potential distribution shows different variations according to increased temperature. Figure 5.16 shows that for constant parti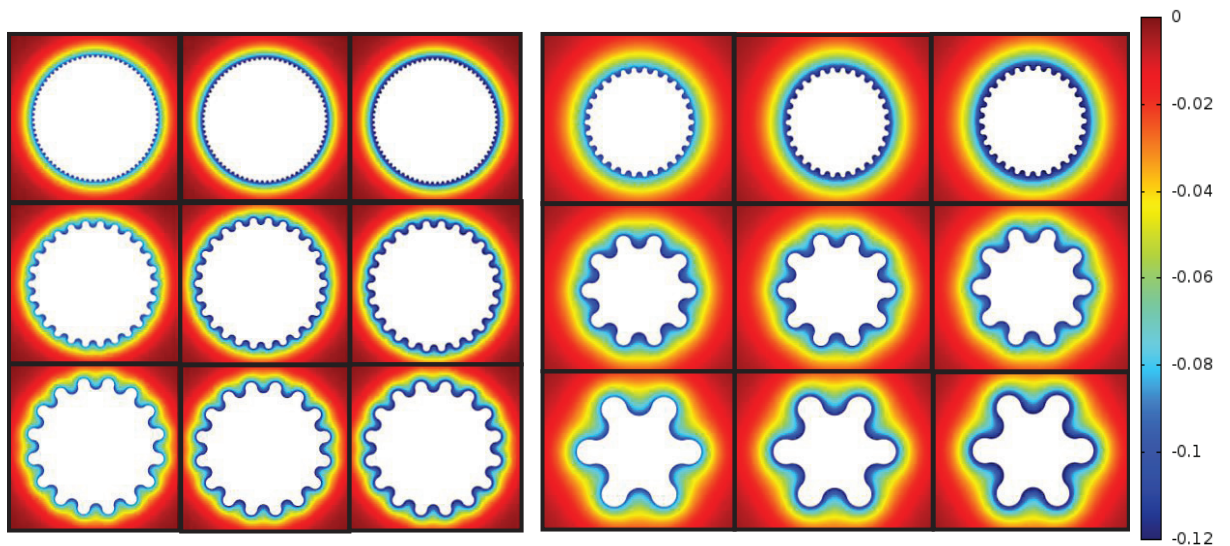cle and roughness diameter when the temperature is increasing electric potential on the surface shows an increasing behavior and electric potential contours that are covered the surface will be getting thicker.

In Figure 5.17, surface charge density distributions are examined more detailed for different particle and roughness diameters. Each graph has a constant particle diameter and shows surface charge variation according to different roughness diameter and temperature values. For instance, in Figure 5.17-a particle diameter is at 20 nm and surface charge density values for each roughness diameter show increasing behavior with increasing temperature.

Figure 5.17. Surface charge density variations according to different temperature values and different nanoparticle and roughness dimensions (D_P=100 nm, T=298, 313, 323 K; D_R=2, 6, 10 nm; D_P=40 nm, T=298, 313, 323 K, D_R=2, 6, 10 nm)

Negative surface charge density increases in magnitude due to the increased temperature. Surface charge density variation is related to ionic distribution on the surface. With increasing, temperature surface concentration of H^+ ions will be decreased and according to that increases the disassociation on the surface. In Figure 5.17-a curvature effect also observed besides temperature and roughness due to the smaller nanoparticle size. On the other hand, in Figure 5.17-c curvature effect will be diminished according to increased particle diameter. It is observed that when particle diameter at this values surface charge density of nanoparticle will reach flat surface theory.

In Figure 5.18 surface charge densities normalized with surface charge density value at 298 K for each particle diameter. The figure shows that normalized surface charge density values increased with increasing temperature according to different roughness diameters. Surface charge densities are changing due to the roughness effect and temperature effect. Roughness structure on the surface will change the ionic distribution through the surface and there is a non-equilibrium ionic region that will appear around the surface. When roughness diameter is increasing electric double layers extending from opposite surfaces will overlap and change the ionic distribution on the gap between roughness. According to that, surface charge density will increase with increasing roughness. Also, when the temperature is increasing ionic distribution on the surface will change. In this figure, we can observe these two main effects on surface charge distribution on the surface.
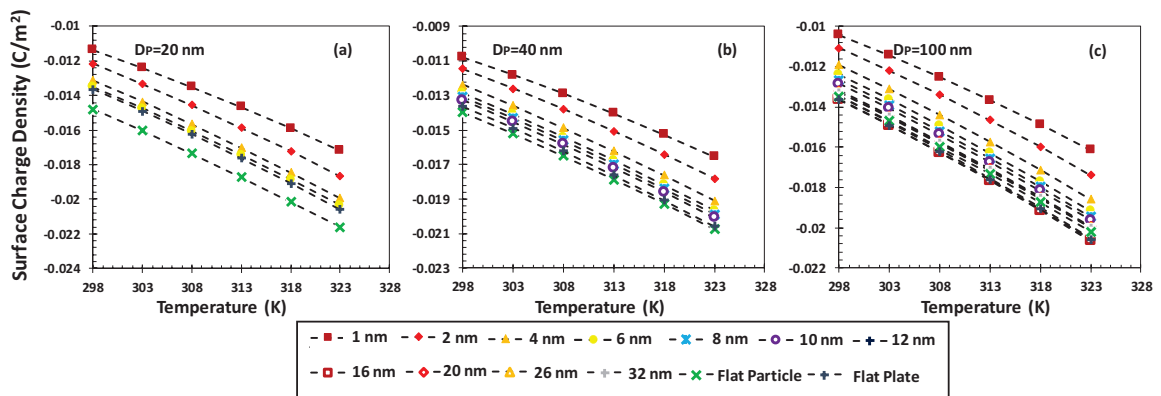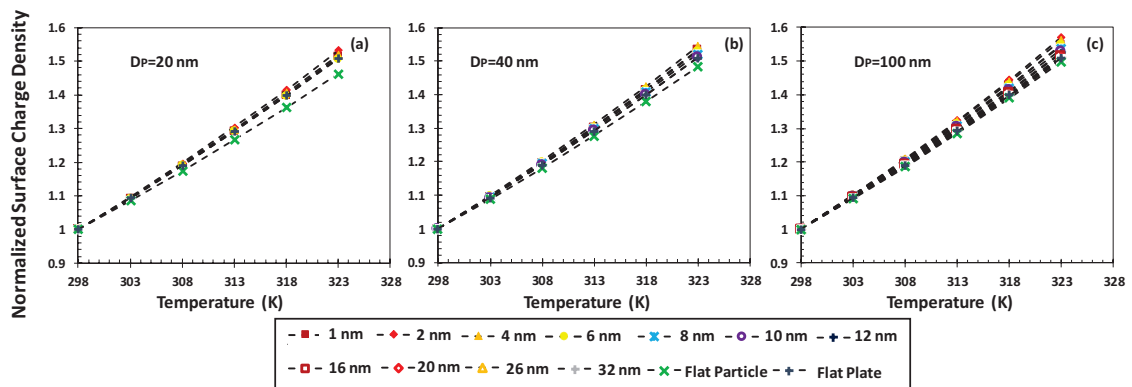

Figure 5.18. Normalized surface charge densities according to different temperature values and different nanoparticle and roughness dimensions (D_P=100 nm, T=298, 313, 323 K; D_R=2,6,10 nm; D_P=40 nm, T=298,313,323 K, D_R=2,6,10 nm)

In Figure 5.19, roughness diameter is kept constant at 6 nm and particle diameter and temperature show variation. Identical roughness diameter is chosen for all particle diameters which are investigated in this study. Owing to that, surface roughness kept the same for all cases and only particle diameter and temperature show variation. Figure 5.19-a shows surface charge density variation according to different temperature and particle diameter. In Figure 5.19-b surface charge density values normalized with surface charge density at 298 K for each particle size. Figure 5.19 shows that by increasing temperature negative surface charge density shows increasing behavior in magnitude. In addition to

that surface, charge shows variation due to the particle size. When the particle diameter is decreasing surface charge density will increase as a magnitude.
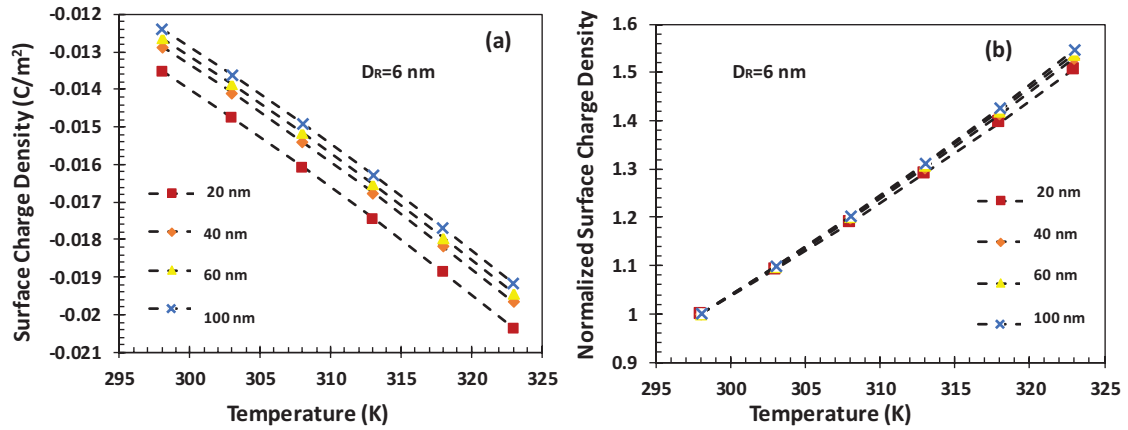
Figure 5.19. Surface charge density variations for different temperature values and different nanoparticle diameters at constant roughness diameter (D_P=20, 40, 60, 100 nm, T=298,313,323 K; D_R=6 nm)

Concentration change also investigated in this step. In Figure 5.20 particle diameter is kept constant at 100 nm and we chose three roughness diameters 2, 10, 26 nm to examine. Particle diameter was chosen at 100 nm because the curvature effect occurring at small particle diameters diminishes and ensures that other effects will be more significant. Because at a critical particle diameter curvature effect will be no longer observed and surface charge density of a particle will reach flat surface theory value.

Also, electrolyte solution concentration was chosen as 0.1, 10 mM, and temperature range is between 298-323 K. When electrolyte concentration is increasing the surface concentration of counter-ions (K^+-Na^+) increases and H^+ ions will be repelled and surface concentration of H^+ decreased.

As a result, the dissociation at the nanoparticle surface increases with increasing concentration. This leads to higher negative surface charge density. When a solution concentration is lower (0.1 mM) surface charge density variation with temperature difference is more significant than at the higher solution concentration (10 mM). Also, surface charge densities are normalized with surface charge density value at 298 K for each particle diameter and concentration condition.
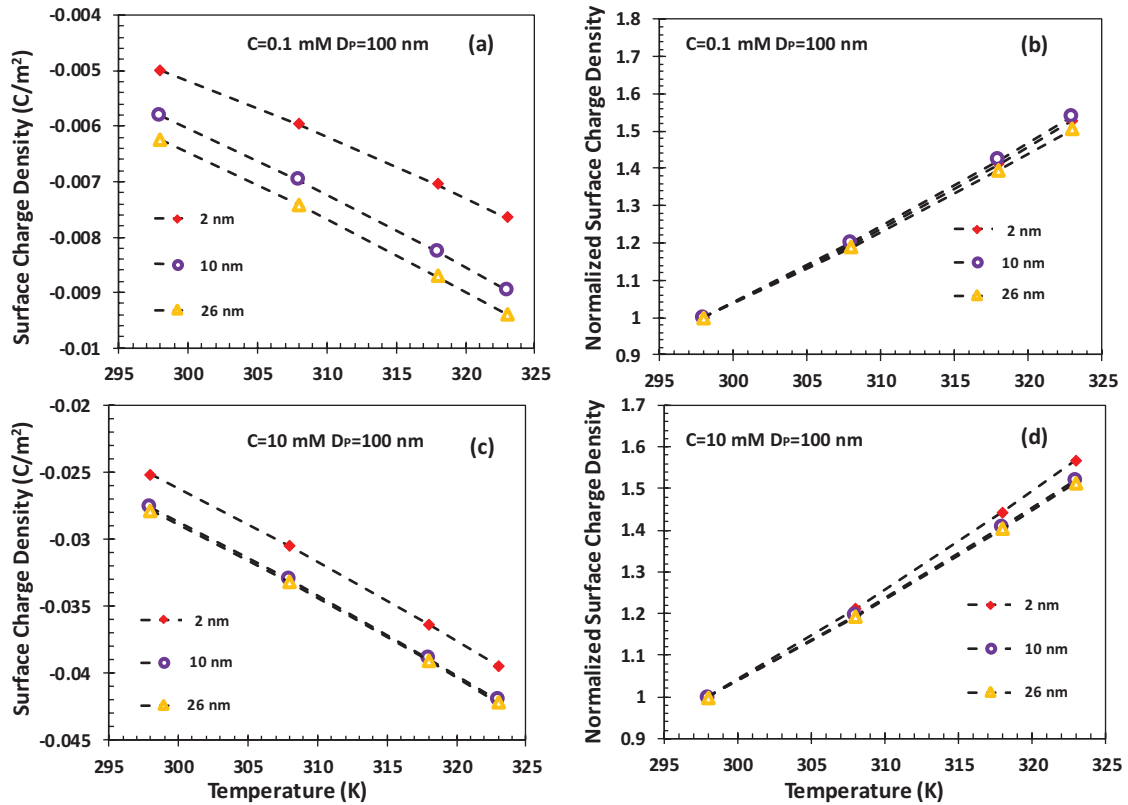
Figure 5.20. Electric potential contour plots according to different temperature values and different nanoparticle and roughness dimensions (D_P=100 nm, T=298,313,323 K; D_R=2,6,10 nm; D_P=40 nm, T=298,313,323 K, D_R=2,6,10 nm)

5.3. Effect of Interaction with a Flat Plate

In this study, surface charge variation of rough nanoparticle when a nanoparticle surface is approaching to a flat surface was investigated. For this purpose, pH = 7.5 and the distance between the particle and the surface were kept constant by selecting R_P + 5 nm from the center of the nanoparticle. Variation of electrical charging was investigated by selecting different particle and pore sizes and solution concentration.

Figure 5.21 shows the variation of the electrical potential distribution on the surface of a rough nanoparticle according to different solution concentrations and particle and roughness diameters. The main reason for the variation of electrical properties of rough nanoparticle surface is that the ionic distribution between flat surface and nanoparticle changes due to the overlapping of electric double layers during an interaction with a flat surface.
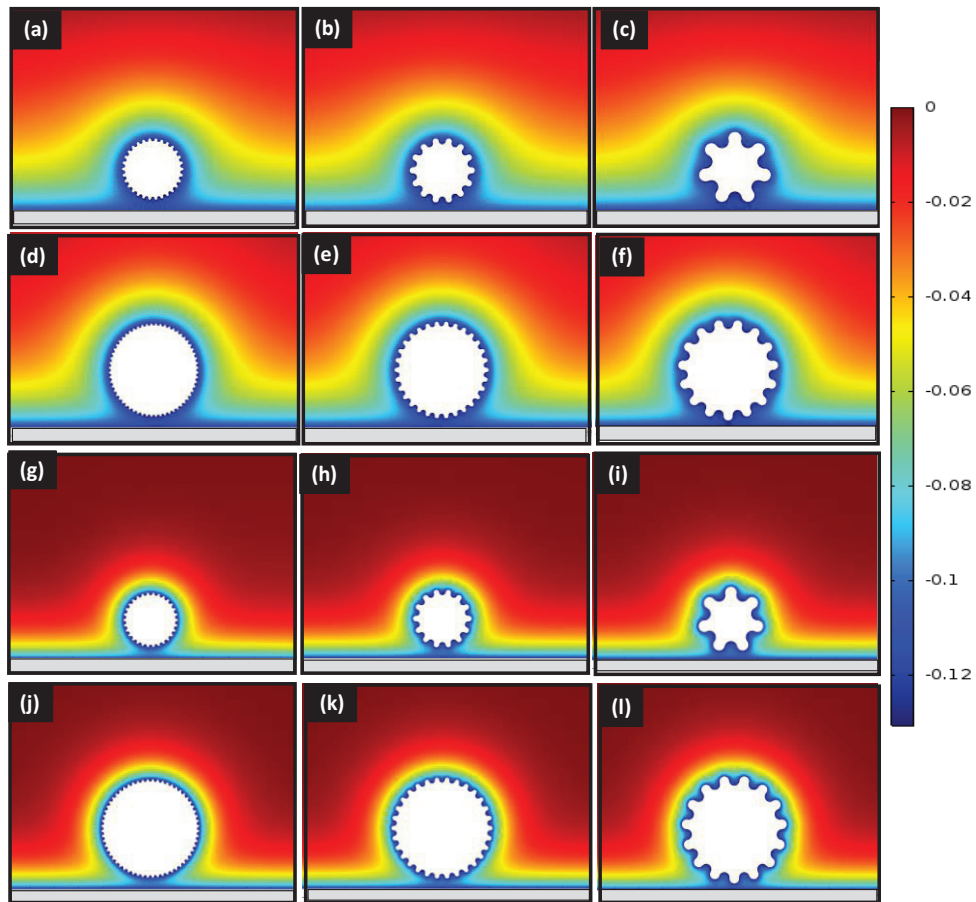
Figure 5.21. Electrical potential distributions on the surface of a rough nanoparticle interacting with a flat plate according to different particle and roughness diameter and concentration values (C=0.1 mM, pH=7.5, Seperation Distance= R_P +5 nm D_P=20 nm a) D_R=1 nm, b) D_R=2 nm, c) D_R=4nm; D_P=40 nm d) D_R=1 nm, e) D_R=2 nm, f) D_R=4 nm; C=1 mM, pH=7.5, D_P=20 nm g) D_R=1 nm, h) D_R=2 nm, i) D_R=4nm; D_P=40 nm j) D_R=1 nm, k) D_R=2 nm, l) D_R=4 nm)

Therefore, it is observed that the ionic distribution of the rough nanoparticle surface which is interacting with a flat plate differs noticeably compared to the non-interacting region of the rough nanoparticle surface. The ionic distribution between the rough nanoparticle and the flat surface results in the formation of an electrostatic force, resulting in a pressure difference between the non-interacting region of nanoparticle surface and interacting region of the nanoparticle surface.

The distribution of the electric potential in the interacting region between the rough nanoparticle and the flat surface as a result of the electrical double layers overlapping with the approach of the nanoparticle to the flat surface differs according to the top region of the nanoparticle.

Figure 5.22. Normalized surface charge distributions on the surface of a rough nanoparticle that interact with a flat surface according to different particle diameter and concentration values (C=0.1 mM,1 mM, pH=7.5, Separation Distance= R_P +5 nm D_P=20 nm-D_R=1 nm, D_P=40 nm-D_R=1 nm,)

There is a greater electric potential occurs at the interacting bottom region of the rough nanoparticle surface. In addition, the roughness of the nanoparticle surface affects the distribution of electrical potential as it changes the ionic distribution on the surface locally.

As a next step, a 180-degree angular surface was defined counterclockwise with reference to the bottom region of the rough nanoparticle surface in order to make a more detailed examination. The surface charge distribution on the rough nanoparticle surface from 0 ° to 180 ° is given in Figure 5.22.

Different particle diameters (20, 40 nm) and concentrations (0.1, 1 mM) were selected by keeping the roughness diameter constant at 1 nm. In addition, the surface charge distribution on the flat surface on which is interacting with a rough nanoparticle is given in the following two graphs. As a result of the interaction of the rough

nanoparticle with a flat surface, the electrical double layers are overlapped. The distribution of positively charged ions increases as a result of being negatively charged on both surfaces in the gap between the rough nanoparticle and the flat surface. As the distribution of positively charged ions increases in the interaction zone, the dissociation from the surface decreases and the negative surface charge decreases.

The surface charge distribution in the interaction zone is lower than the distribution on the non-interacting surface of the rough nanoparticle. As can be seen in the graph, the normalized surface charge distribution on the surface of the rough nanoparticle deviates from the theory as it approaches the interaction region and decreases as it approaches the non-interacting region of the surface. Similarly, the normalized surface charge distribution calculated on the flat surface deviates from the theory as it approaches the interaction region. However, while moving away from the interaction region and approaching the non-interacting region where there is no interaction of the flat surface, it is seen that the normalized surface charge approaches to 1. In addition, as the concentration of solution increases, the distribution of positive ions in the interaction region changes and the surface charge distribution decreases.

A similar examination was repeated for a larger roughness diameter (D_R= 4 nm). When normalized surface charge distributions are examined for a larger roughness diameter, the deviation in the interaction region is more apparent.

As a result of this, the ionic distribution changes and the surface charge distribution increases with increasing roughness. Therefore, the change in surface charge distribution was observed more clearly as we approached the interaction region. Similarly, the surface charge distribution on the nanoparticle approaches the theory as it moves away from the interaction region. For the flat surface, the surface charge distribution deviates from the theory as it approaches the interaction region.

After that, in order to observe in more detail, the variation of surface charge distribution between the downward region of the rough nanoparticle which interacts with the flat surface and the non-interacting upward region, the surface charge was examined by measuring locally. The surface charge distributions measured separately from the upward and downward regions of the rough nanoparticle were normalized with flat surface values. It is observed that the normalized surface charge distribution is lower in the downward region of the nanoparticle where it interacts with the flat surface. It is higher on the non-interacting region of the surface and the normalized surface charge distributions increase with increasing roughness in both regions. When roughness

diameter is increasing both of the normalized surface charge values of the top and bottom regions show an increasing behavior.
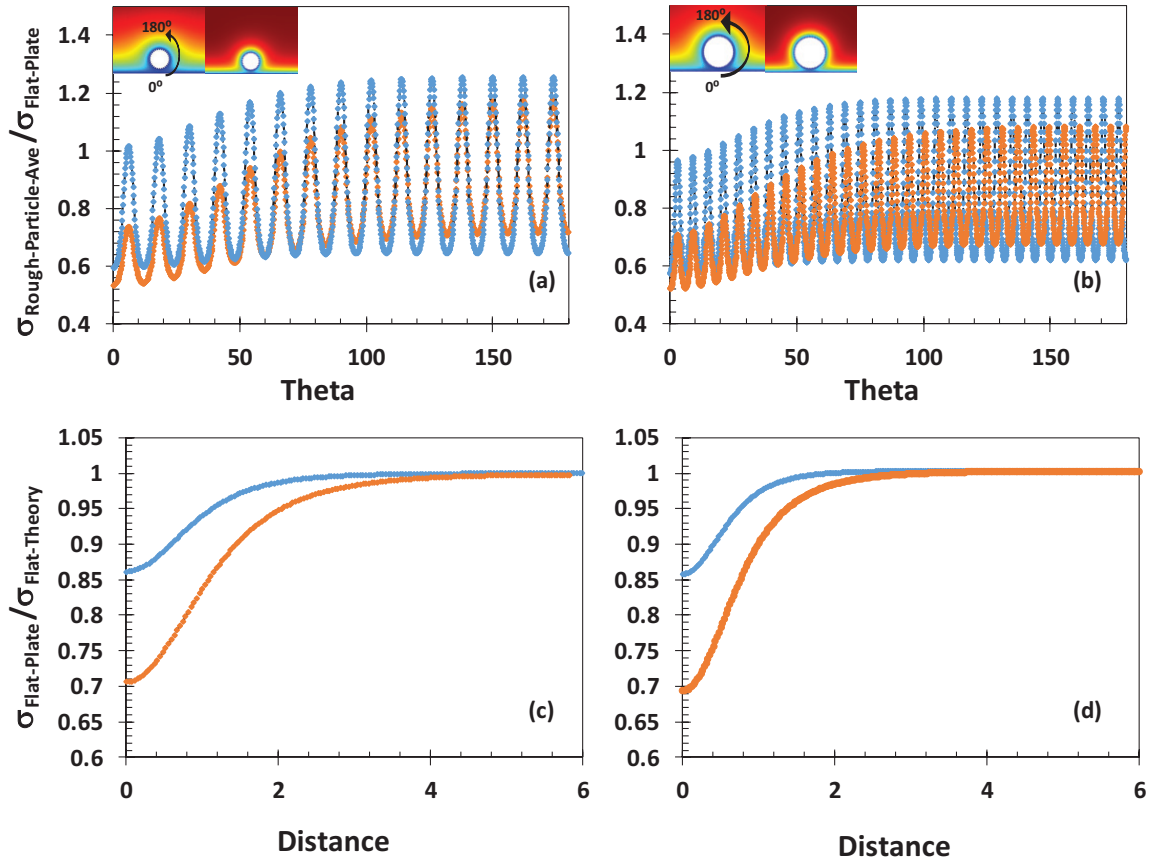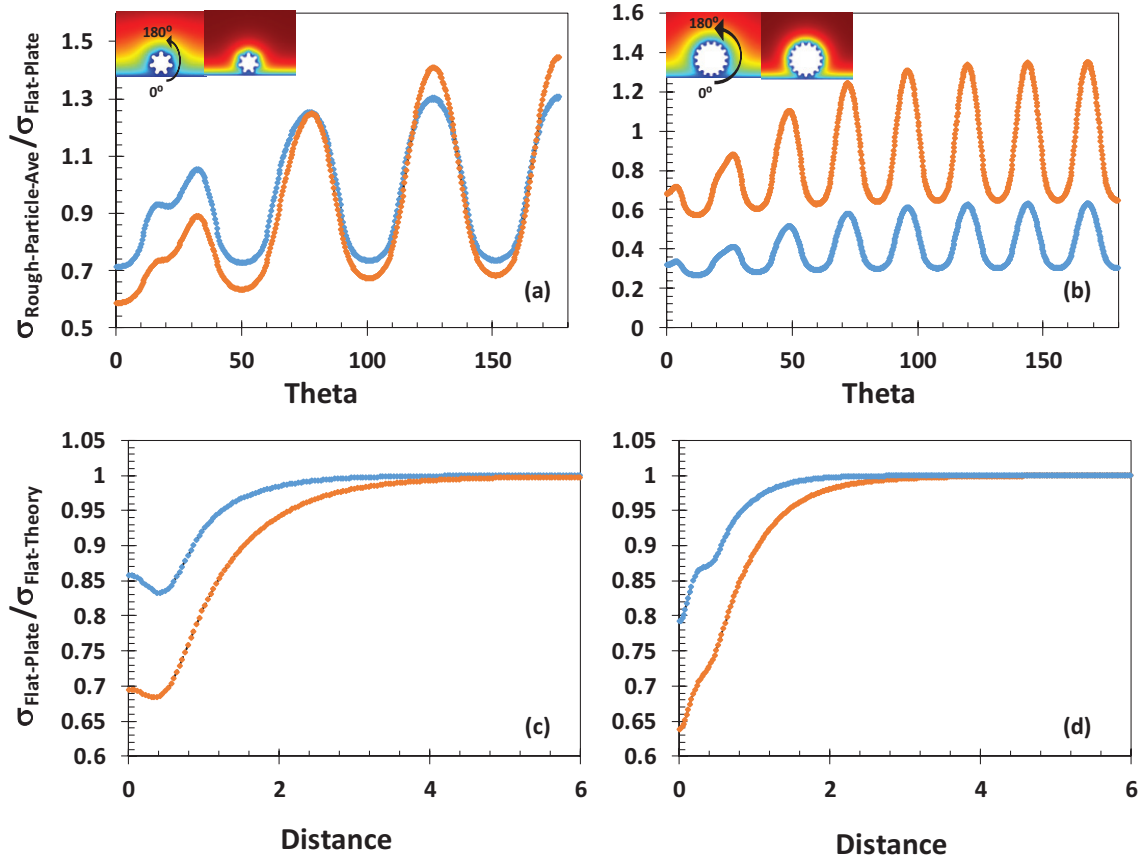

Figure 5.23. Normalized surface charge distributions on the surface of a rough nanoparticle that interact with a flat surface according to different particle diameter and concentration values (C=0.1 mM,1 mM, pH=7.5, Separation Distance= R_P +5 nm D_P=20 nm-D_R=4 nm, D_P=40 nm-D_R=4 nm,)

In the next step, the surface charge distribution values measured from the top and bottom surfaces of the nanoparticle were normalized with the surface charge values of a rough nanoparticle during the non-interacting case and having an equivalent diameter with the particle diameter.

The reason for this is to ensure that the surface charge variation during the interaction of the rough nanoparticle with a flat surface is examined without the effect of particle and roughness diameter (curvature and EDL overlap).
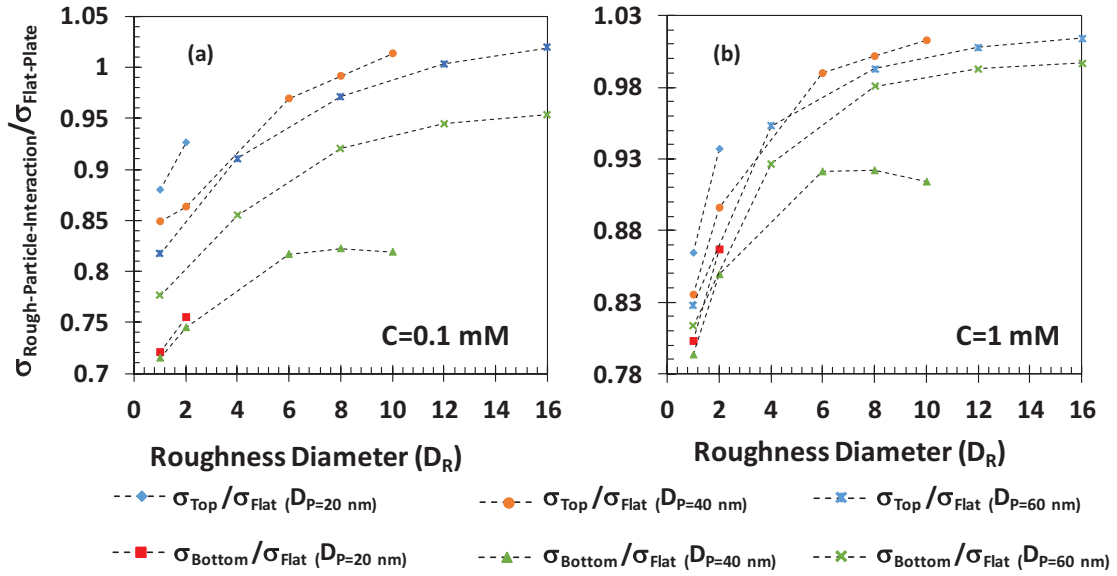
Figure 5.24. Normalized surface charge distributions from the top and bottom of the surface of a rough nanoparticle which interact with a flat surface according to different particle diameter and concentration values (C=0.1 mM,1 mM, pH=7.5, Separation Distance= R_P +5 nm D_P=20 nm-D_R=1 nm, 2 nm; D_P=40 nm-D_R=1 nm, 2 nm, 6 nm, 8 nm, 10nm; D_P=60 nm-D_R=1 nm, 4 nm, 8 nm, 12 nm, 16 nm)

Here, it is seen that different surface charge distribution occurs between the bottom surface interacting with the flat surface and the non-interacting top region of the surface of the nanoparticle. The normalized surface charge distribution on the top region of the nanoparticle surface is fixed at around 1 and stabilized with an increasing roughness diameter. In contrast, the normalized surface charge distribution on the bottom region of the nanoparticle surface shows an increasing behavior with an increasing roughness diameter for interaction cases. We can see that interaction with a flat surface is changing surface charge distribution on an interaction region of nanoparticle surface. As the solution concentration increases, the increase in the normalized surface charge distribution related to variable ionic concentration on the interaction zone is more significant.

Here, surface charge distributions are examined locally for the top (non-interaction region) and bottom (interaction region) regions of the nanoparticle surface because when a rough nanoparticle is interacting with a flat surface there is a pressure difference is occurred in the interaction region of a nanoparticle surface. This pressure difference is observed due to the different ionic concentrations in the interaction region

because when a nanoparticle is interacting with a surface electric double layers extending from opposite surfaces are overlapped and this formation increases the ionic distribution on the interaction region.
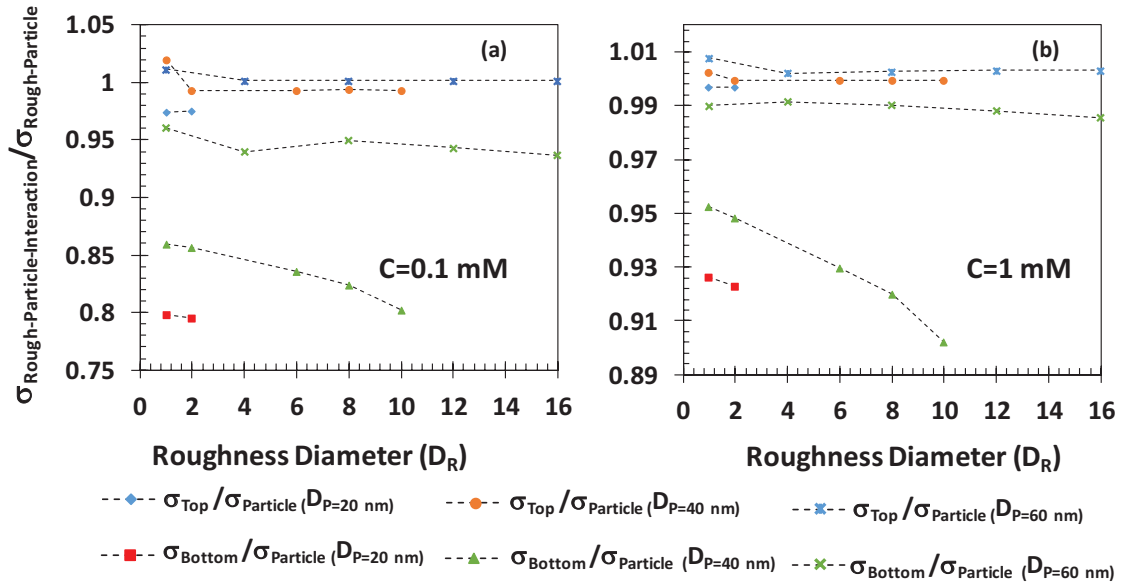
Figure 5.25. Normalized surface charge distributions of a particle (with the surface charge of non-interacting nanoparticle having a similar roughness diameter and particle diameter) taken from the top and bottom regions of a rough nanoparticle surface interacting with a flat surface according to different particle and roughness diameter (C=0.1 mM,1 mM, pH=7.5, Separation Distance= R_P +5 nm D_P=20 nm-D_R=1 nm, 2 nm; D_P=40 nm-D_R=1 nm, 2 nm, 6 nm, 8 nm, 10nm; D_P=60 nm-D_R=1 nm, 4 nm, 8 nm, 12 nm, 16 nm)

As a result, there is a pressure difference occurs and surface charge density is changed. According to that pressure difference, there is a force formed between the nanoparticle surface and flat surface. This force is formed with pressure difference and included electric double layer force which is formed due to the varied ionic concentration. So, we attempt to investigate the surface charging behavior of a rough nanoparticle during an interaction with a surface according to examine this force that occurred on a nanoparticle surface as a future study.

CHAPTER 6

DISCUSSION

The surface charging behavior of silica nanoparticles is very important for diverse application areas such as colloidal science, surface science, biomedical applications, and electrokinetic transport. Surface charge density variation of silica nanoparticles needs to be investigated under different surface conditions such as pH, electrolyte concentration, roughness and particle diameter, the temperature of the ionic medium and interaction effect with other surfaces. When a nanoparticle immersed in an aqueous media there is a protonation/deprotonation surface reactions occur solid/liquid interface. The surface charge will be formed on the nanoparticle surface due to these protonation/deprotonation reactions and adsorption of ions. Charged nanoparticle will attract counter-ions and repel co-ions. As a result, an ionic distribution will be formed on the particle surface. The electric double layer will be formed according to this behavior. Generally, ionic distribution on the surface is defined with Boltzmann-Distribution. However, Boltzmann-Distribution is not valid for our case (zeta potential must be smaller than 25 mV and surface must be sufficiently away from other surfaces) and instead of Boltzmann-Distribution, the Nernst-Planck equation is implemented in the solution to define ionic transport. The Poisson equation gives electric potential distribution. Poisson-Nernst Planck equation was used to solve coupled for calculating surface charge behavior of nanoparticle. Also, the charge regulation model used as a boundary condition of the surface because constant potential or constant charge models cannot be used for this case. This is because both surface charge and electric potential show variation and they are related to each other. In this study, PNP equations solved numerically and the charge regulation model is implemented as a boundary condition to calculate surface charge densities of nanoparticles.

The aim of this study was to investigate the surface charging behavior of nanoparticles under different surface conditions. First, varied particle and roughness diameters were chosen and thus, different geometrical structures obtained on the surface of the nanoparticle. Rough structures on the nanoparticle formed a geometrical structure including hills and pits. There was a gap formed between two roughness geometry and

electric double layer extending from opposite surfaces will overlap and ionic concentration in this gap will change locally. EDL overlapping is a very important effect occurred due to the roughness effect. Also, the curvature effect is another important factor which occurs due to the increasing roughness and particle diameters and affected surface charging behavior. When roughness diameter is increasing surface charge density on the surface shows an increasing behavior and it is becoming similar to the flat surface theory. Because the EDL overlap effect will decrease with increasing roughness diameter. In contrast, when roughness diameter decreases surface charge density differs from the flat surface theory. This is because with decreasing roughness diameter, protrusions on the particle surface becoming smaller than the EDL thickness. Accordingly, EDLs extending from surfaces of roughness geometries on the surface will overlap and surface charge differs from the flat surface. Also, there is a curvature effect occurs due to that decreasing particle diameter. The average surface charge density will increase with decreased particle diameter. Two of most important effects occur on the nanoparticle surface, curvature effect and EDL overlap effect. These two conditions are very important and effective on surface charge density formation on the nanoparticle surface. Curvature effect occurs due to the decreased diameter and EDL overlap occurs due to decreased roughness diameter. We investigated the variation of surface charge densities of rough nanoparticles also under different pH and electrolyte concentrations. The surface charge was highly dependent on electrolyte solution conditions. Also, surface charge density was affected by pH variation. When the pH level increases, the bulk concentration of H+ ions decreases. Because of that H^+ concentration on the rough nanoparticle surface resulted in a lower concentration. Surface charge density will have higher values due to the difference in ionic concentration on the surface. The effect of pH variation is more effective in cases with smaller roughness diameter. This behavior can be seen due to the EDL overlap effect. EDL overlap is more dominant for smaller roughness diameters. Surface charge density variation with different pH levels examined using different characterization parameters but there is not a proper explanation that can be found about pH effect on surface charging behavior. In order to achieve this, there is an empirical model defined that is explain the surface charging behavior of rough nanoparticle according to different pH.

In the second step, the temperature difference added to the model. When the temperature is changing relative permittivity of ionic media, ionic diffusivities of ions and equilibrium constants of surface chemical reactions will change. The variation of

these parameters according to temperature defined with proper equations found in the literature. Surface charge density variation is investigated under temperature difference. When the temperature is increasing negative surface charge density increases in magnitude. Surface charge density changes because of the different ionic distribution on the surface. Ionic distribution on the surface will change with increasing temperature because when the temperature increases, the surface concentration of H^+ ions will be decreased and disassociation on the surface will increase. Also, different electrolyte solution was chosen for investigating temperature effect. When electrolyte concentration is increasing the surface concentrations of counter-ions (K^+ -Na^+) increases and for this reason, H^+ ions will be repelled and concentration of H^+ decreased. When the electrolyte solution increases, the dissociation at the nanoparticle surface will increase. Due to that, higher negative surface charge density will be formed on the nanoparticle surface. When solution concentration is lower surface charge density variation with temperature difference is more significant than at the higher solution concentration.

As a next step, the surface charge of a rough nanoparticle was examined during rough nanoparticle interacting with a flat plate. When two dielectric objects interact with each other in an aqueous solution their electric double layers will overlap and in the gap between these objects ionic properties of the solution will change. There is a non-uniform ionic distribution occurring on the surface of rough nanoparticle when particle interacting with other surfaces. According to non-uniform ionic distribution, non-uniform surface charging will be formed on the surface of the particle. Surface charging of rough nanoparticle investigated under different roughness and particle diameters and solution concentrations when the separation distance between the rough nanoparticle and flat surface is kept constant. When a rough nanoparticle interacts with a flat surface the electric double layers extending from surfaces will be overlapped. The distribution of positively charged ions increases in the gap between the rough nanoparticle and the flat surface resulting in both of the surfaces being negatively charged. As the distribution of positively charged ions increases in the interaction zone, the dissociation from the surface decreases and the negative surface charge decreases. The surface charge distribution in the interaction zone is lower than the distribution on the non-interacting region of the surface of the rough nanoparticle. Surface charge distribution on the surface of the rough nanoparticle deviates from the theory as it approaches the interaction region and decreases as it approaches the non-interacting region of the surface.

REFERENCES

(1)   Liong, M.; Lu, J.; Kovochich, M.; Xia, T.; Ruehm, S. G.; Nel, A. E.; Tamanoi, F.; Zink, J. I. Multifunctional Inorganic Nanoparticles for Imaging, Targeting, and Drug Delivery. *ACS Nano* **2008**. https://doi.org/10.1021/nn800072t.

(2)   Lee, J. E.; Lee, N.; Kim, T.; Kim, J.; Hyeon, T. Multifunctional Mesoporous Silica Nanocomposite Nanoparticles for Theranostic Applications. *Acc. Chem. Res.* **2011**. https://doi.org/10.1021/ar2000259.

(3)   Slowing, I. I.; Trewyn, B. G.; Giri, S.; Lin, V. S. Y. Mesoporous Silica Nanoparticles for Drug Delivery and Biosensing Applications. *Adv. Funct. Mater.* **2007**. https://doi.org/10.1002/adfm.200601191.

(4)   Popat, A.; Hartono, S. B.; Stahr, F.; Liu, J.; Qiao, S. Z.; Lu, G. Q. Mesoporous Silica Nanoparticles for Bioadsorption, Enzyme Immobilisation, and Delivery Carriers. *Nanoscale*. **2011**. https://doi.org/10.1039/c1nr10224a.

(5)   Naito, M.; Abe, H.; Yamauchi, Y.; Ji, Q.; Mori, T.; Ariga, K.; Hill, J. P. Enzyme Nanoarchitectonics: Organization and Device Application. *Chem. Soc. Rev.* **2013**. https://doi.org/10.1039/c2cs35475f.

(6)   Li, Z.; Barnes, J. C.; Bosoy, A.; Stoddart, J. F.; Zink, J. I. Mesoporous Silica Nanoparticles in Biomedical Applications. *Chemical Society Reviews*. **2012**. https://doi.org/10.1039/c1cs15246g.

(7)   Vivero-Escoto, J. L.; Slowing, I. I.; Lin, V. S. Y.; Trewyn, B. G. Mesoporous Silica Nanoparticles for Intracellular Controlled Drug Delivery. *Small*. **2010**. https://doi.org/10.1002/smll.200901789.

(8)   Yang, P.; Gai, S.; Lin, J. Functionalized Mesoporous Silica Materials for Controlled Drug Delivery. *Chemical Society Reviews*. **2012**. https://doi.org/10.1039/c2cs15308d.

(9)   Li, X.; Xie, Q. R.; Zhang, J.; Xia, W.; Gu, H. The Packaging of SiRNA within the Mesoporous Structure of Silica Nanoparticles. *Biomaterials* **2011**. https://doi.org/10.1016/j.biomaterials.2011.08.068.

(10)   Xiao, D.; Jia, H. Z.; Ma, N.; Zhuo, R. X.; Zhang, X. Z. A Redox-Responsive Mesoporous Silica Nanoparticle Capped with Amphiphilic Peptides by Self-Assembly for Cancer Targeting Drug Delivery. *Nanoscale* **2015**. https://doi.org/10.1039/c5nr02247a.

(11) Perrault, S. D.; Walkey, C.; Jennings, T.; Fischer, H. C.; Chan, W. C. W. Mediating Tumor Targeting Efficiency of Nanoparticles through Design. *Nano Lett.* **2009**. https://doi.org/10.1021/nl900031y.

(12) Cho, K.; Wang, X.; Nie, S.; Chen, Z.; Shin, D. M. Therapeutic Nanoparticles for Drug Delivery in Cancer. *Clinical Cancer Research*. **2008**. https://doi.org/10.1158/1078-0432.CCR-07-1441.

(13) Barisik, M.; Atalay, S.; Beskok, A.; Qian, S. Size Dependent Surface Charge Properties of Silica Nanoparticles. *J. Phys. Chem. C* **2014**, *118* (4), 1836–1842. https://doi.org/10.1021/jp410536n.

(14) Argyo, C.; Weiss, V.; Bräuchle, C.; Bein, T. Multifunctional Mesoporous Silica Nanoparticles as a Universal Platform for Drug Delivery. *Chemistry of Materials*. **2014**. https://doi.org/10.1021/cm402592t.

(15) Slowing, I.; Trewyn, B. G.; Lin, V. S. Y. Effect of Surface Functionalization of MCM-41-Type Mesoporous Silica Nanoparticles on the Endocytosis by Human Cancer Cells. *J. Am. Chem. Soc.* **2006**. https://doi.org/10.1021/ja0645943.

(16) Forest, V.; Cottier, M.; Pourchez, J. Electrostatic Interactions Favor the Binding of Positive Nanoparticles on Cells: A Reductive Theory. *Nano Today* **2015**. https://doi.org/10.1016/j.nantod.2015.07.002.

(17) Shang, L.; Nienhaus, K.; Nienhaus, G. U. Engineered Nanoparticles Interacting with Cells: Size Matters. *Journal of Nanobiotechnology*. **2014**. https://doi.org/10.1186/1477-3155-12-5.

(18) Koike, N.; Chaikittisilp, W.; Shimojima, A.; Okubo, T. Surfactant-Free Synthesis of Hollow Mesoporous Organosilica Nanoparticles with Controllable Particle Sizes and Diversified Organic Moieties. *RSC Adv.* **2016**. https://doi.org/10.1039/c6ra22926c.

(19) Kang, J. S.; Lim, J.; Rho, W. Y.; Kim, J.; Moon, D. S.; Jeong, J.; Jung, D.; Choi, J. W.; Lee, J. K.; Sung, Y. E. Wrinkled Silica/Titania Nanoparticles with Tunable Interwrinkle Distances for Efficient Utilization of Photons in Dye-Sensitized Solar Cells. *Sci. Rep.* **2016**. https://doi.org/10.1038/srep30829.

(20) Shi, Y. R.; Ye, M. P.; Du, L. C.; Weng, Y. X. Experimental Determination of Particle Size-Dependent Surface Charge Density for Silica Nanospheres. *J. Phys. Chem. C* **2018**. https://doi.org/10.1021/acs.jpcc.8b07566.

(21) Ninham, B. W.; Parsegian, V. A. Electrostatic Potential between Surfaces Bearing Ionizable Groups in Ionic Equilibrium with Physiologic Saline Solution.

J. Theor. Biol. **1971**. https://doi.org/10.1016/0022-5193(71)90019-1.

(22) Shubin, V. E.; Kékicheff, P. Electrical Double Layer Structure Revisited via a
Surface Force Apparatus: Mica Interfaces in Lithium Nitrate Solutions. *J. Colloid
Interface Sci.* **1993**. https://doi.org/10.1006/jcis.1993.1016.

(23) Chapel, J. P. Electrolyte Species Dependent Hydration Forces between Silica
Surfaces. *Langmuir* **1994**. https://doi.org/10.1021/la00023a053.

(24) Dishon, M.; Zohar, O.; Sivan, U. From Repulsion to Attraction and Back to
Repulsion: The Effect of NaCl, KCl, and CsCl on the Force between Silica
Surfaces in Aqueous Solution. *Langmuir* **2009**.
https://doi.org/10.1021/la803022b.

(25) Popa, I.; Sinha, P.; Finessi, M.; Maroni, P.; Papastavrou, G.; Borkovec, M.
Importance of Charge Regulation in Attractive Double-Layer Forces between
Dissimilar Surfaces. *Phys. Rev. Lett.* **2010**.
https://doi.org/10.1103/PhysRevLett.104.228301.

(26) Hughes, C.; Yeh, L. H.; Qian, S. Field Effect Modulation of Surface Charge
Property and Electroosmotic Flow in a Nanochannel: Stern Layer Effect. *J. Phys.
Chem. C* **2013**. https://doi.org/10.1021/jp402018u.

(27) Trefalt, G.; Behrens, S. H.; Borkovec, M. Charge Regulation in the Electrical
Double Layer: Ion Adsorption and Surface Interactions. *Langmuir* **2016**.
https://doi.org/10.1021/acs.langmuir.5b03611.

(28) Ozcelik, H. G.; Barisik, M. Electric Charge of Nanopatterned Silica Surfaces.
Phys. Chem. Chem. Phys. **2019**. https://doi.org/10.1039/c9cp00706g.

(29) Taghipoor, M.; Bertsch, A.; Renaud, P. Thermal Control of Ionic Transport and
Fluid Flow in Nanofluidic Channels. *Nanoscale* **2015**, *7* (44), 18799–18804.
https://doi.org/10.1039/c5nr05409e.

(30) Taghipoor, M.; Bertsch, A.; Renaud, P. Temperature Sensitivity of Nanochannel
Electrical Conductance. *ACS Nano* **2015**, *9* (4), 4563–4571.
https://doi.org/10.1021/acsnano.5b01196.

(31) Hsu, J. P.; Tai, Y. H.; Yeh, L. H.; Tseng, S. Importance of Temperature Effect on
the Electrophoretic Behavior of Charge-Regulated Particles. *Langmuir* **2012**, *28*
(1), 1013–1019. https://doi.org/10.1021/la203245n.

(32) Tang, G. Y.; Yang, C.; Gong, H. Q.; Chai, J. C.; Lam, Y. C. Numerical
Simulation of Joule Heating Effect on Sample Band Transport in Capillary
Electrophoresis. *Anal. Chim. Acta* **2006**, *561* (1–2), 138–149.

https://doi.org/10.1016/j.aca.2005.12.068.

(33)   Kresge, C. T.; Leonowicz, M. E.; Roth, W. J.; Vartuli, J. C.; Beck, J. S. Ordered Mesoporous Molecular Sieves Synthesized by a Liquid-Crystal Template Mechanism. *Nature* **1992**. https://doi.org/10.1038/359710a0.

(34)   Inagaki, S.; Fukushima, Y.; Kuroda, K. Synthesis of Highly Ordered Mesoporous Materials from a Layered Polysilicate. *J. Chem. Soc. Chem. Commun.* **1993**. https://doi.org/10.1039/C39930000680.

(35)   Beck, J. S.; Vartuli, J. C.; Roth, W. J.; Leonowicz, M. E.; Kresge, C. T.; Schmitt, K. D.; Chu, C. T. W.; Olson, D. H.; Sheppard, E. W.; McCullen, S. B.; et al. A New Family of Mesoporous Molecular Sieves Prepared with Liquid Crystal Templates. *J. Am. Chem. Soc.* **1992**. https://doi.org/10.1021/ja00053a020.

(36)   Trewyn, B. G.; Slowing, I. I.; Giri, S.; Chen, H. T.; Lin, V. S. Y. Synthesis and Functionalization of a Mesoporous Silica Nanoparticle Based on the Sol-Gel Process and Applications in Controlled Release. *Accounts of Chemical Research*. **2007**. https://doi.org/10.1021/ar600032u.

(37)   Øye, G.; Sjöblom, J.; Stöcker, M. Synthesis, Characterization and Potential Applications of New Materials in the Mesoporous Range. *Adv. Colloid Interface Sci.* **2001**. https://doi.org/10.1016/S0001-8686(00)00066-X.

(38)   Zhao, D.; Huo, Q.; Feng, J.; Chmelka, B. F.; Stucky, G. D. Nonionic Triblock and Star Diblock Copolymer and Oligomeric Sufactant Syntheses of Highly Ordered, Hydrothermally Stable, Mesoporous Silica Structures. *J. Am. Chem. Soc.* **1998**. https://doi.org/10.1021/ja974025i.

(39)   Wang, W.; Wang, P.; Tang, X.; Elzatahry, A. A.; Wang, S.; Al-Dahyan, D.; Zhao, M.; Yao, C.; Hung, C. Te; Zhu, X.; et al. Facile Synthesis of Uniform Virus-like Mesoporous Silica Nanoparticles for Enhanced Cellular Internalization. *ACS Cent. Sci.* **2017**. https://doi.org/10.1021/acscentsci.7b00257.

(40)   Niu, Y.; Yu, M.; Hartono, S. B.; Yang, J.; Xu, H.; Zhang, H.; Zhang, J.; Zou, J.; Dexter, A.; Gu, W.; et al. Nanoparticles Mimicking Viral Surface Topography for Enhanced Cellular Delivery. *Adv. Mater.* **2013**. https://doi.org/10.1002/adma.201302737.

(41)   Cho, E. C.; Xie, J.; Wurm, P. A.; Xia, Y. Understanding the Role of Surface Charges in Cellular Adsorption versus Internalization by Selectively Removing Gold Nanoparticles on the Cell Surface with a I 2/KI Etchant. *Nano Lett.* **2009**. https://doi.org/10.1021/nl803487r.

(42) Lu, F.; Wu, S.-H.; Hung, Y.; Mou, C.-Y. Size Effect on Cell Uptake in Well-Suspended, Uniform Mesoporous Silica Nanoparticles. *Small* **2009**. https://doi.org/10.1002/smll.200900005.

(43) Pan, L.; He, Q.; Liu, J.; Chen, Y.; Ma, M.; Zhang, L.; Shi, J. Nuclear-Targeted Drug Delivery of Tat Peptide-Conjugated Monodisperse Mesoporous Silica Nanoparticles. *J. Am. Chem. Soc.* **2012**. https://doi.org/10.1021/ja211035w.

(44) Kim, H. L.; Lee, S. B.; Jeong, H. J.; Kim, D. W. Enhanced Tumor Targetability of PEGylated Mesoporous Silica Nanoparticles on in Vivo Optical Imaging According to Their Size. *RSC Adv.* **2014**. https://doi.org/10.1039/c4ra03905j.

(45) Gan, Q.; Dai, D.; Yuan, Y.; Qian, J.; Sha, S.; Shi, J.; Liu, C. Effect of Size on the Cellular Endocytosis and Controlled Release of Mesoporous Silica Nanoparticles for Intracellular Delivery. *Biomed. Microdevices* **2012**. https://doi.org/10.1007/s10544-011-9604-9.

(46) Slowing, I.; Trewyn, B. G.; Lin, V. S. Y. Effect of Surface Functionalization of MCM-41-Type Mesoporous Silica Nanoparticles on the Endocytosis by Human Cancer Cells. *J. Am. Chem. Soc.* **2006**. https://doi.org/10.1021/ja0645943.

(47) Florek, J.; Caillard, R.; Kleitz, F. Evaluation of Mesoporous Silica Nanoparticles for Oral Drug Delivery-Current Status and Perspective of MSNs Drug Carriers. *Nanoscale* **2017**. https://doi.org/10.1039/c7nr05762h.

(48) Bouchoucha, M.; Côté, M. F.; C-Gaudreault, R.; Fortin, M. A.; Kleitz, F. Size-Controlled Functionalized Mesoporous Silica Nanoparticles for Tunable Drug Release and Enhanced Anti-Tumoral Activity. *Chem. Mater.* **2016**. https://doi.org/10.1021/acs.chemmater.6b00877.

(49) Evenhuis, C. J.; Haddad, P. R. Joule Heating Effects and the Experimental Determination of Temperature during CE. *Electrophoresis* **2009**, *30* (5), 897–909. https://doi.org/10.1002/elps.200800643.

(50) Seyrek, E.; Dubin, P. L.; Newkome, G. R. Effect of Electric Field on the Mobility of Carboxyl-Terminated Dendrimers. *J. Phys. Chem. B* **2007**, *108* (28), 10168–10171. https://doi.org/10.1021/jp0380071.

(51) Wang, C. K.; Tsao, H. K. Temperature-Insensitive Electrokinetic Behavior in Capillary Zone Electrophoresis. *J. Phys. Chem. B* **2004**, *108* (45), 17685–17693. https://doi.org/10.1021/jp0472156.

(52) Evenhuis, C. J.; Hruska, V.; Guijt, R. M.; Macka, M.; Gaš, B.; Marriott, P. J.; Haddad, P. R. Reliable Electrophoretic Mobilities Free from Joule Heating

Effects Using CE. *Electrophoresis* **2007**, *28* (20), 3759–3766. https://doi.org/10.1002/elps.200700343.

(53) Xuan, X.; Li, D. Analytical Study of Joule Heating Effects on Electrokinetic Transportation in Capillary Electrophoresis. *J. Chromatogr. A* **2005**, *1064* (2), 227–237. https://doi.org/10.1016/j.chroma.2004.12.033.

(54) Tseng, S.; Li, Y. M.; Lin, C. Y.; Hsu, J. P. Salinity Gradient Power: Influences of Temperature and Nanopore Size. *Nanoscale* **2016**, *8* (4), 2350–2357. https://doi.org/10.1039/c5nr07563g.

(55) Hwang, J.; Sekimoto, T.; Hsu, W. L.; Kataoka, S.; Endo, A.; Daiguji, H. Thermal Dependence of Nanofluidic Energy Conversion by Reverse Electrodialysis. *Nanoscale* **2017**, *9* (33), 12068–12076. https://doi.org/10.1039/c7nr04387b.

(56) Bianchi, E.; van Oostrum, P. D. J.; Likos, C. N.; Kahl, G. Inverse Patchy Colloids: Synthesis, Modeling and Self-Organization. *Current Opinion in Colloid and Interface Science*. **2017**. https://doi.org/10.1016/j.cocis.2017.03.010.

(57) Stroock, A. D.; Whitesides, G. M. Controlling Flows in Microchannels with Patterned Surface Charge and Topography. *Accounts of Chemical Research*. 2003. https://doi.org/10.1021/ar0202870.

(58) Borghi, F.; Vyas, V.; Podestà, A.; Milani, P. Nanoscale Roughness and Morphology Affect the IsoElectric Point of Titania Surfaces. *PLoS One* **2013**. https://doi.org/10.1371/journal.pone.0068655.

(59) Duval, J. F. L.; Leermakers, F. A. M.; Van Leeuwen, H. P. Electrostatic Interactions between Double Layers: Influence of Surface Roughness, Regulation, and Chemical Heterogeneities. *Langmuir* **2004**. https://doi.org/10.1021/la030404f.

(60) Nosrati, R.; Hadigol, M.; Raisee, M.; Nourbakhsh, A. Numerical Modeling of Electroosmotic Nanoflows with Overlapped Electric Double Layer. *J. Comput. Theor. Nanosci.* **2012**. https://doi.org/10.1166/jctn.2012.2643.

(61) Huang, K. Da; Yang, R. J. Electrokinetic Behaviour of Overlapped Electric Double Layers in Nanofluidic Channels. *Nanotechnology* **2007**, *18* (11). https://doi.org/10.1088/0957-4484/18/11/115701.

(62) Karniadakis, G.; Beskok, A.; Aluru, N. Microflows and Nanoflows. Springer, New York **2005**.

(63) Li, D. *Electrokinetics In Microfluidics*; Elsevier/Academic Press, **2004**.

(64) Hunter, R. *Zeta Potential In Colloid Science*; Academic Press: London, **1981**.

(65) Qian, S.; Ai, Y. *Electrokinetic Particle Transport In Micro-/Nanofluidics*; CRC Press: Boca Raton, **2012**.

(66) Oh, Y.-J.; Garcia, A. L.; Petsev, D. N.; Lopez, G. P.; Brueck, S. R. J.; Ivory, C. F.; Han, S. M. Effect of Wall–Molecule Interactions on Electrokinetic Transport of Charged Molecules in Nanofluidic Channels during FET Flow Control. *Lab Chip* **2009**, *9* (11), 1601. https://doi.org/10.1039/b901382m.

(67) Zhang, M.; Yeh, L. H.; Qian, S.; Hsu, J. P.; Joo, S. W. DNA Electrokinetic Translocation through a Nanopore: Local Permittivity Environment Effect. *J. Phys. Chem. C* **2012**, *116* (7), 4793–4801. https://doi.org/10.1021/jp211798x.

(68) Jing, D.; Bhushan, B. Electroviscous Effect on Fluid Drag in a Microchannel with Large Zeta Potential. *Beilstein J. Nanotechnol.* **2015**, *6* (1), 2207–2216. https://doi.org/10.3762/bjnano.6.226.

(69) Sefcik, J.; Goddard, W. A. Thermochemistry of Silicic Acid Deprotonation: Comparison of Gas-Phase and Solvated DFT Calculations to Experiment. *Geochim. Cosmochim. Acta* **2001**, *65* (24), 4435–4443. https://doi.org/10.1016/S0016-7037(01)00739-6.

(70) Hiemstra, T.; De Wit, J. C. .; Van Riemsdijk, W. . Multisite Proton Adsorption Modeling at the Solid/Solution Interface of (Hydr)Oxides: A New Approach. *J. Colloid Interface Sci.* **2004**, *133* (1), 105–117. https://doi.org/10.1016/0021-9797(89)90285-3.

(71) Hsu, J. P.; Huang, C. H.; Tseng, S. Influence of Temperature on the Gel Electrophoresis of a PH-Regulated, Zwitterionic Sphere. *Soft Matter* **2013**, *9* (48), 11534–11541. https://doi.org/10.1039/c3sm52406j.

(72) Hsu, C.; Lo, T. W.; Lee, D. J.; Hsu, J. P. Electrophoresis of a Charge-Regulated Zwitterionic Particle: Influence of Temperature and Bulk Salt Concentration. *Langmuir* **2013**, *29* (7), 2427–2433. https://doi.org/10.1021/la3047752.

(73) Owen, B. B.; Miller, R. C.; Milner, C. E.; Cogan, H. L. The Dielectric Constant of Water As a Function of Temperature and Pressure 1,2 . *J. Phys. Chem.* **2007**, *65* (11), 2065–2070. https://doi.org/10.1021/j100828a035.

(74) Kaatze, U. Complex Permittivity of Water as a Function of Frequency and Temperature. *J. Chem. Eng. Data* **1989**, *34* (4), 371–374. https://doi.org/10.1021/je00058a001.

(75) Tseng, S.; Lin, J. Y.; Hsu, J. P. Theoretical Study of Temperature Influence on the Electrophoresis of a PH-Regulated Polyelectrolyte. *Anal. Chim. Acta* **2014**,

847, 80–89. https://doi.org/10.1016/j.aca.2014.08.045.

(76)   Poling, B. E.; Prausnitz, J. M.; O'Connel, J. P. *The Properties of Gases and Liquids*; **2009**; Vol. 12. https://doi.org/10.1063/1.3060771.

(77)   Biswas, R.; Bagchi, B. Limiting Ionic Conductance of Symmetrical, Rigid Ions in Aqueous Solutions: Temperature Dependence and Solvent Isotope Effects. *J. Am. Chem. Soc.* **1997**, *119* (25), 5946–5953. https://doi.org/10.1021/ja970118o.

(78)   The Physical Chemistry of ELECTROLYTIC SOLUTIONS. *Chem. Eng. News* **2010**. https://doi.org/10.1021/cen-v036n004a.p059.

(79)   Haynes, W. M. *CRC Handbook of Chemistry and Physics, 95th Edition, 2014-2015*; **2014**. https://doi.org/10.1136/oem.53.7.504.

(80)   Robinson, R. A.; Stokes, R. H. *Electrolyte Solutions: Second Revised Edition*; **2002**.

(81)   Zhuravlev, L. T. Surface Characterization of Amorphous Silica-a Review of Work from the Former USSR. *Colloids Surfaces A Physicochem. Eng. Asp.* **1993**. https://doi.org/10.1016/0927-7757(93)80399-Y.

(82)   Brown, M. A.; Abbas, Z.; Kleibert, A.; Green, R. G.; Goel, A.; May, S.; Squires, T. M. Determination of Surface Potential and Electrical Double-Layer Structure at the Aqueous Electrolyte-Nanoparticle Interface. *Phys. Rev. X* **2016**. https://doi.org/10.1103/PhysRevX.6.011007.

(83)   Rodriguez-Santiago, V.; Fedkin, M. V.; Lvov, S. N. Electrophoresis System for High Temperature Mobility Measurements of Nanosize Particles. *Rev. Sci. Instrum.* **2008**. https://doi.org/10.1063/1.2976779.